UNIVERSITY OF TARTU
Faculty of Science and Technology
Institute of Physics

Anna Maria Tuberg

# ATOMIC LAYER DEPOSITION AND PROPERTIES OF GALLIUM AND TIN OXIDE-BASED THIN FILMS

**Master's Thesis (30 EAP)**

Curriculum 'Materials Science and Technology'

Supervisors:
PhD Lauri Aarik
PhD Kaupo Kukli

Tartu 2025

## ATOMIC LAYER DEPOSITION AND PROPERTIES OF GALLIUM AND TIN OXIDE-BASED THIN FILMS

Thin films are the backbone of modern industries and the drivers of next-generation technological innovations. In this thesis, gallium and tin oxide based thin films and heterostructures were studied. The films were synthesised by atomic layer deposition using $GaI_3$-$O_3$ and $SnI_4$-$O_3$ as precursors. The growth, elemental and phase composition of the films were analysed and correlations between those and the optical and electrical properties were investigated. The study showed that the growth rates of $Ga_2O_3$ and $SnO_2$ depended on the surface and starting from certain layer thicknesses, the thin films did not mix but formed smooth layered heterostructures. The optical and electrical properties depended on the composition and structure of the films, where a significant effect was seen for resistivity values of the thin films. The work demonstrates that materials with improved properties can be prepared by mixing gallium and tin oxide.

**Keywords:** Atomic layer deposition, gallium oxide, tin oxide, heterostructures, thin films

**CERCS codes and names: T150** Material technology; **T155** Coatings and surface treatment; **P265** Semiconductor physics.

## GALLIUM- JA TINAOKSIIDIL PÕHINEVATE AATOMKIHTSADESTATUD KILEDE OMADUSED

Õhukesed kiled ja struktuurid on kasutuses igas kaasaegses tööstusharus ning on uue põlvkonna tehnoloogiliste uuenduste eestvedajad. Selles magistritöös uuriti aatomkihtsadestusmeetodiga valmistatud $Ga_2O_3$ ja $SnO_2$-l põhinevaid ühe- ja mitmekihilisti struktuure, kus lähteainetena kasutati $GaI_3$-$O_3$ ja $SnI_4$-$O_3$. Selleks viidi läbi kilede kasvu, koostise ja struktuurianalüüs ning uuriti, kuidas tulemused mõjutasid materjali optilisi ja elektrilisi omadusi. Tulemused näitasid, et $Ga_2O_3$ ja $SnO_2$ kasvukiirused sõltusid kasvualusest. Lisaks nähti, et alates teatud paksusest, õhukestest kihtidest koosnev struktuur ei segunenud, vaid moodustus õhukestest siledastest kihtidest koosnev heterostruktuur. Mõõdetud optilised ja elektrilised omadused olenesid kilede koostisest ning struktuurist, millede muutumise korral oli suurt mõju näha just kilede eritakistuste väärtustele. Töö näitab, et gallium- ja tinaoksiidi omavahelisel segamisel on võimalik valmistada parendatud omadustega materjale.

**Võtmesõnad:** Aatomkihtsadestus, galliumoksiid, tinaoksiid, heterostruktuurid, õhukesed kiled

**CERCS koodid ja nimetused: T150** Materjalitehnoloogia; **T155** Pinded ja pinnatehnoloogia; **P265** Pooljuhtide füüsika.

# TABLE OF CONTENTS

ABBREVIATIONS ........ 4
1 INTRODUCTION ........ 5
2 LITERATURE OVERVIEW ........ 9
2.1 Atomic Layer Deposition ........ 9
2.2 Deposition of ternary compounds using ALD ........ 10
2.3 Thin Film Characterization Techniques ........ 11
2.3.1 Real-Time Characterization of Thin Film Growth ........ 11
2.3.2 Composition of the Thin Films ........ 12
2.3.3 Phase Composition Analysis ........ 12
2.3.4 Optical Parameters ........ 14
2.3.5 Electrical Properties ........ 14
3 EXPERIMENTAL PART ........ 15
3.1 Deposition of $Ga_2O_3$, $SnO_2$ and $Ga_2O_3$-$SnO_2$ Based Thin Films ........ 15
3.2 Sample Characterization ........ 16
4 RESULTS AND DISCUSSION ........ 17
4.1 Growth of $Ga_2O_3$ and $SnO_2$ Thin Films ........ 17
4.2 Growth and the Phase Composition of $Ga_2O_3$-$SnO_2$ Thin Films ........ 20
4.3 Optical Properties ........ 25
4.4 Electrical Properties ........ 28
SUMMARY ........ 31
SUMMARY IN ESTONIAN ........ 33
ACKNOWLEDGEMENTS ........ 35
REFERENCES ........ 36
Appendices ........ 42
NON-EXCLUSIVE LICENCE TO REPRODUCE THESIS AND MAKE THESIS PUBLIC ........ 44

# ABBREVIATIONS

| | |
|---|---|
| ALD | Atomic Layer Deposition |
| CVD | Chemical Vapour Deposition |
| XRF | X-Ray Fluorescence |
| XRD | X-Ray Diffraction |
| GIXRD | Grazing-Incidence X-Ray Diffraction |
| XRR | X-Ray Reflectivity |
| SE | Spectroscopic Ellipsometry |
| QCM | Quartz Crystal Microbalance |
| EBE | Electron Beam Evaporation |
| GPC | Growth Per Cycle |
| MGPC | Mass Growth Per Cycle |
| $n$ | Refractive Index |
| $k$ | Extinction Coefficient |
| $\rho$ | Resistivity |
| $Ga_2O_3$ | Gallium (III) Oxide |
| $SnO_2$ | Tin (IV) Oxide |

# 1 INTRODUCTION

Semiconductors shape the future of electronic and optoelectronic technologies and are used in all modern industries [1]. While silicon, the most used semiconductor has been around since the 1950s, its physical constraints have shifted the attention to other materials that withstand environments where Si works inefficiently. These materials are wide band gap (WBG) semiconductors, such as silicon carbide or gallium nitride, that are predicted to surpass the performance of silicon [2]. Interestingly, a fourth-generation WBG compound, gallium oxide has captured interest as the demand for higher-performance and more efficient electronics has grown significantly [3].

Gallium oxide ($Ga_2O_3$) is a WBG semiconductor material with potential applications in gas sensors, high-power and high-voltage electronics and ultraviolet (UV) photodetectors [4]. Furthermore, possibilities of using $Ga_2O_3$ as a photocatalyst for water-splitting have been studied [5, 6]. Its high breakdown voltage [4], superb thermal stability, and deep UV absorption make it a promising material for electronic and optical devices [7].

Previous studies have found that $Ga_2O_3$ has at least 6 polymorphs: corundum α, monoclinic β, spinel γ, cubic δ, hexagonal ε and orthorhombic κ [8]. Among these, β-$Ga_2O_3$ is thermodynamically most stable and has been studied most extensively. However, it has been demonstrated that the properties of $Ga_2O_3$ can largely depend on the crystal structure and phase composition of the deposited thin films [9, 10]. Recently, the metastable phases have started to gain interest due to potentially having superior properties compared to β-$Ga_2O_3$. For instance, α-$Ga_2O_3$ is known for its high density and highest bandgap ($E_g$) values among all phases [11]. Outstanding photocatalysis and luminescent properties are attributed to γ-$Ga_2O_3$ and according to first-principle studies, both κ- and ε-$Ga_2O_3$ phases possess spontaneous polarization and ferroelectric properties suitable for piezoelectric devices [4]. In addition, the densities of κ- and ε-$Ga_2O_3$ are relatively similar to that of α-$Ga_2O_3$, in the range of 5.88 – 6.1 g/cm$^3$ [8, 12]. However, achieving crystalline thin films of metastable $Ga_2O_3$ phase is quite challenging and either annealing or a suitable substrate is needed for the growth. Yet, annealing is not favourable for synthesising metastable $Ga_2O_3$ because most of the phases tend to recrystallize into β-phase upon thermal treatment at approximately 700 °C. Hence, different substrates are used, such as sapphires with different orientations that facilitate the growth of specific metastable phases [13]. Si(100) is another common substrate material that has been used for β-$Ga_2O_3$ deposition

[14, 15]. Nevertheless, little is known about the growth of metastable phases on bare Si(100), so this work aims to fill that void.

Tin oxide ($SnO_2$) is a WBG semiconductor material that has found usage in solar cells, transparent conducting oxides (TCOs), gas sensors, and catalysis [16]. These versatile applications are owing to its beneficial characteristics – $SnO_2$ has a density of 6.95 g/cm$^3$ [17], $E_g$ of approximately 3.6 eV, high transmittance (~85%) [18] and refractive index of approximately 2.05 at 633 nm [19, 20], which can be influenced by deposition methods and parameters [21]. $SnO_2$ is an n-type semiconductor due to interstitial tin atoms and oxygen vacancies and can be easily doped to tune its properties for different applications.

There are multiple methods for preparing $Ga_2O_3$ and $SnO_2$ thin films, for instance, pulsed layer deposition (PLD) [22], metal-organic chemical vapour deposition (MOCVD), radio frequency magnetron sputtering (RFMS) [23] and atomic layer deposition (ALD) [12, 19]. Among these methods, ALD is favoured for its remarkably effective control over the film composition, which allows efficient study of the influence of doping of various materials on their properties [24]. Intentional doping is a method that is used to tailor the properties of a material for various applications. In the case of semiconductors, electrical, optical, and structural properties are commonly enhanced. In this work, the influence of doping on material properties is studied by varying the cation concentration in the gallium-tin-oxide (GTO) based thin films. For that, two recently introduced precursor combinations for ALD – $GaI_3$-$O_3$ and $SnI_4$-$O_3$ – are used, in which case the only impurity element in the films can be iodine.

Knowing the optical parameters of the transparent oxides and their dependence on the wavelength of light is crucial for engineering optoelectronic devices [25]. Depending on the phase, $Ga_2O_3$ can have $E_g$ in the range of 4.0 – 5.6 eV. The refractive index $n$ can vary from 1.7 – 1.9 for amorphous films, 1.96 for κ/ε-$Ga_2O_3$ [12] and 1.68 – 1.89 for β-$Ga_2O_3$ [8, 26]. Interestingly, these properties can be enhanced by incorporating Sn into $Ga_2O_3$. However, only a few studies have been conducted about the effect of Sn doping on $Ga_2O_3$ $n$ values, specifically [27, 29]. *Shen et al* [28] reported that the content of Sn in the $Ga_2O_3$ thin films is a major factor that affects their refractive indices, where they noticed that $n$ value decreased when increasing the level of Sn. On the contrary, film with 50% Sn content had the highest $n$ value, which was thought to be due to the $SnO_2$ phase emerging at high Sn concentrations. The extinction coefficient ($k$) of a material is a key factor in the fabrication of optoelectronic devices as it shows the amount of energy loss of light in the films [30]. As $k$ becomes zero from a specific

wavelength, the material exhibits almost full transparency. Previously, *Shen et al* also found that the $k$ of $Ga_2O_3$ became larger as the doping level of Sn increased and close to zero values were observed from 340 nm wavelength. Evidently, the findings confirm doping as a viable method for adjusting the optical properties.

The introduction of impurities is the most used technique for altering the conductivity of semiconductors [31]. Control over the electrical properties is a crucial aspect of semiconducting oxides as their conductivity affects the range of suitable applications. $Ga_2O_3$ has an intrinsic n-type conductivity and is generally classified as a highly resistive semiconductor [32]. However, numerous studies have shown that its conductivity can be effectively tuned through doping or by altering the growth parameters. For instance, *Zhang et al* [22] showed that the resistivity ($\rho$) of β-$Ga_2O_3$ could be varied from $10^2$ to $10^5$ Ω×cm just by adjusting the oxygen and nitrogen pressures during PLD. Nevertheless, doping has become the primary method for modifying electrical properties. Mainly group IV elements, such as Si, Ge and Sn are used as external dopants [33], but elements including Fe, Nb, Ta, Al [33] and Zn [34] have also been studied. *Zhang et al* [35] reported that using Fe as a dopant increased the $\rho$ up to $2.63\times10^{11}$ Ω×cm, resulting in an insulating material. However, low resistivity is preferable for applications that need large electric currents, such as UV-transparent electrodes for UV light-emitting diodes [36]. In previous work, *Parisini et al* [9] presented low resistivity values for Si- and Sn-doped ε-$Ga_2O_3$ thin films – 1 and 10 Ω×cm, respectively. Furthermore, *Vijayan et al* [27] saw that the conductivity of β-$Ga_2O_3$ single crystals increased up to 21.4 $(\Omega\times cm)^{-1}$ when doped with Sn (up to 20 wt%). Additionally, a decrease of resistivity by almost 10 orders of magnitude was demonstrated by increasing the concentration of Sn from 1% to 10%, according to *Mi et al* [37]. However, raising the Sn concentration above 10% showed increasing resistivity values, which were thought to emerge due to lower crystalline quality and charge carrier scattering from the defects.

Various elements have been studied for $SnO_2$ doping, such as Fe, Ni [38], Ga [39], and In [40]. In-doped $SnO_2$ is a widely used material in TCOs, displays, solar cells etc [40], owing to enhanced optical and electrical properties [41]. Similarly to In, Ga is a IIIA group element and they both act as acceptors if they occupy a Sn site in the lattice, theoretically leading to an improved carrier conductivity [42, 43]. In a previous study by *Sivakumar et al* [39], the sheet resistance and electrical resistivity of Ga-doped $SnO_2$ thin films were analysed. It was found that the sheet resistance and resistivity increased with growing Ga content due to the increasing number of grain boundaries and electron traps. Furthermore, the effect of In and Ga doping

concentration on $SnO_2$ resistivity has been studied by *Mogilatenko et al* [44]. It was seen that at certain Ga doping concentrations, the resistivity of $SnO_2$ increased by a few orders of magnitude. The phenomena were thought to arise due to the compensation of donors by Ga acceptors. Further increasing the concentration led to the formation of secondary phases, lowering the resistivity. These results demonstrate that doping is a feasible method for altering the properties of thin films.

Binary gallium oxide thin films have potential applications in high-power electronics, TCO's and optoelectronic devices. However, the use of non-doped $Ga_2O_3$ is limited by its low conductivity, relatively small range of light absorption and difficulty in synthesising metastable phases. Hence, this master's thesis aimed to analyse how the composition of gallium and tin oxide influence the growth and structural, optical, and electrical properties of the thin films. Particularly, it focused on the properties of $\kappa$-$Ga_2O_3$ and $\varepsilon$-$Ga_2O_3$ phases that have been studied to a markedly lesser extent than the $\beta$-$Ga_2O_3$ phase. The first goal of the thesis was to analyse the effect of Sn concentration on phase composition and crystallinity of doped $Ga_2O_3$ thin films and $Ga_2O_3$-$SnO_x$-based (GTO) heterostructures. The second objective was to evaluate the influence of Sn-doping on the refractive index and extinction coefficient. Lastly, this thesis aimed to investigate the impact of Sn concentration on the thin films' resistivity.

In this work, the author contributed to the preparation of the thin films by placing samples into the chamber, taking them out and using the ALD control software. The author took part in the characterisation of the films' growth, composition, structure and optical parameters of binary $Ga_2O_3$, $SnO_2$, and GTO thin films using quartz crystal microbalance, X-ray fluorescence, X-ray diffraction, X-ray reflectivity and spectroscopic ellipsometry. With these methods, the author placed the samples into the devices, used control software and analysed the obtained data. The surface resistivity values of the thin films were evaluated by measuring the voltage function of the distance with 4 probes, where the author had their part in setting up the right measurement configuration, using LABVIEW software, measuring the voltages and analysing obtained data.

The first section of the thesis gives an overview of the used materials and their properties. ALD principles and material characterization methods are described in the second part. The third section gives an outline of the thin film deposition and sample characterization parameters. The fourth section presents the results and analysis of the findings, followed by the summary in the fifth part.

# 2 LITERATURE OVERVIEW

## 2.1 Atomic Layer Deposition

Atomic layer deposition is a chemical vapour deposition method based on a self-limiting reaction of two or more gaseous precursors at a solid sample surface, allowing to deposit thin films with atomic thicknesses, high quality and superb repeatability. One of the main advantages of ALD is that it is not confined to only 2D substrates but is rather efficient in covering complex 3D shapes in a uniform material layer as well [45–48]. Consequently, ALD has found its purpose in a vast range of applications, varying from microelectronics to medical coatings [49]. The atomic layer deposition technique was patented by Dr. Tuomo Suntola and colleagues in the 1970s, when there was a need for thin films in flat-panel displays [50]. Nowadays, ALD has developed into an invaluable method and is vastly used for depositing dielectric and metal films. In addition, different 3D structures, for instance transistor gates and nanoporous surfaces can be fabricated with it [46]. In the energy industry, ALD is used for solar cells, fuel cells, and batteries for the deposition of different barriers and conducting thin films [50, 51]. In optical applications, ALD enables to deposit thin films that are used as antireflection or high-reflection coatings [52].

The deposition of a material layer takes place in a stepwise manner (Fig. 1) [46]. An ALD cycle consists of four major processes. Firstly, one of the precursors is introduced into the ALD chamber, where it reacts with the sample surface until the surface saturates. Secondly, the excess precursor and by-products are purged by an inert carrier gas. Thirdly, the second precursor is pumped into the chamber, where it reacts with the sample surface and activates it so the first precursor can react with it again. Fourthly, the by-products and non-reacted material are purged again, preparing the surface for the next cycle. This way, a part of the monolayer is formed, where after each cycle the surface is covered with the same functional groups as in the beginning, allowing to repeat the cycle. As all these steps are self-limiting on the surface, the processes can be cycled until a needed thickness of the thin film has been reached [42, 49].

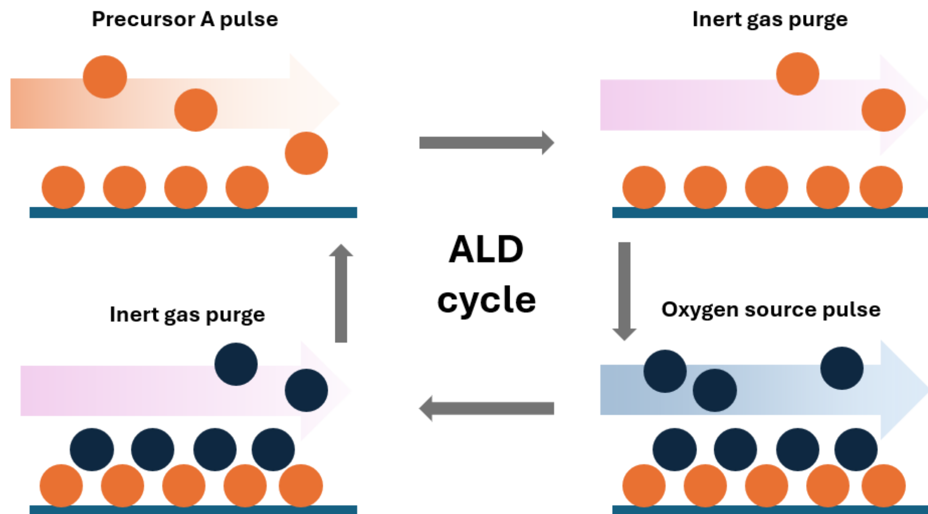


**Figure 1**. A scheme of atomic layer deposition cycle processes.

## 2.2 Deposition of ternary compounds using ALD

Atomic layer deposition of semiconductive oxides with more than one metal precursors has become a subject of interest for its ability to control the doping level and composition of deposited films [53]. Doping is used to tune the properties of the host material. The effect of tuning depends on the dopant content and can have different effects at low and high concentrations. Low concentrations are typically used to enhance the optoelectronic properties, while high concentrations can significantly change the crystallinity and band structure of the films.

When the number of cycles for the dopant precursor is a lot smaller compared to the host precursor material, the dopant atoms are more likely to mix into the structure of host material, resulting in a doped material [53]. Contrary to doping, superlattices can arise when the number of the precursor materials cycles is comparably large, which promotes the formation of discrete, sequentially alternating layers. The layered structure gives the possibility to regulate structural, optical, and electrical properties [54, 55]. ALD-based Sn-doping of $Ga_2O_3$ has been extensively studied, while the formation and characterization of different GTO heterostructures and superlattices has been investigated significantly less [56, 57].

## 2.3 Thin Film Characterization Techniques

The evaluation of the functional properties of $SnO_2$, $Ga_2O_3$ and GTO thin films was done using different characterization methods. These techniques provide a comprehensive overview of the films' structural, optical, and electrical behaviours and give an understanding of the influence of doping concentration and growth conditions on the film properties.

### *2.3.1 Real-Time Characterization of Thin Film Growth*

Real-time characterization of the ALD process is used to tune the deposition parameters to optimize the quality of the thin films and the efficiency of the deposition process [58]. Mostly, Spectroscopic Ellipsometry (SE) [59], Fourier Transform Infrared Spectroscopy (FTIR) [60], X-ray Photoelectron Spectroscopy (XPS) [61], Quadrupole Mass Spectroscopy (QMS) [62], and Quartz Crystal Microbalance (QCM) [63] methods have been employed.

In this work, the ALD process and thin film growth were characterized by the QCM method. QCM is based on a piezoelectric effect arising from the changes in the oscillation of a quartz crystal when a mass is deposited onto the crystal's surface. From the decrease of the oscillation frequency, the deposited mass quantity can be measured [64]. QCM also allows for analysis of the precursor adsorption and desorption at the surface, which can be observed from the mass changes ($\Delta m_1$ and $\Delta m_2$ in Fig. 2). The overall mass growth during one growth cycle can be determined as $\Delta m_1$ - $\Delta m_2$.

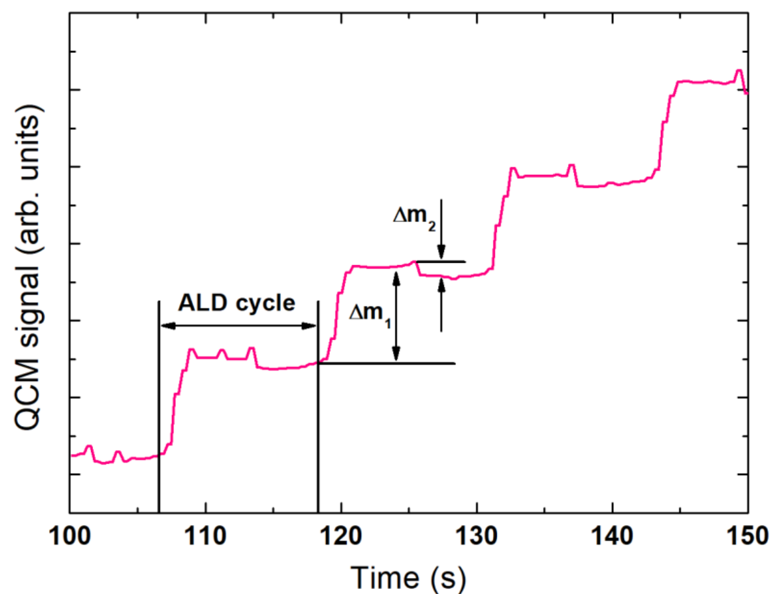


**Figure 2**. QCM signal as a function of time in $GaI_3$-$O_3$ ALD process.

### *2.3.2 Composition of the Thin Films*

The elemental composition of thin films can be characterized with various methods, such as energy dispersive X-ray spectroscopy (EDX), XPS [65], and X-ray fluorescence (XRF) [63].

In this thesis, the composition of deposited thin films was analysed with XRF. It is a non-destructive method based on measuring the emitted fluorescent X-rays that emerge during the interaction between radiation and a material. The incident radiation can have energy high enough to eject electrons from the inner orbitals of an atom, making it unstable. To return to its lowest energy state, a higher orbital electron falls to the inner orbital and releases energy equal to the difference between the two orbitals. Since the released energy is characteristic of every element, we can measure the emitted secondary X-rays and associate them with specific elements [66]. In addition to qualitative analysis, XRF also allows quantitative analysis, where the measured radiation is converted into elemental concentrations [67].

### *2.3.3 Phase Composition Analysis*

Information about the phase composition, crystal structure and crystallinity of thin films can be obtained with various techniques, for instance Raman spectroscopy [68], XRD [63, 65], X-ray Reflectivity (XRR) [28], Grazing Incidence X-ray diffraction (GIXRD) [12], and Reflection High-Energy Electron Diffraction (RHEED) [69].

When radiation with a wavelength similar to the distance between crystal planes interacts with a material, the radiation scatters and creates rays that interfere with each other in either a destructive or constructive manner, also known as diffraction. Diffraction takes place mostly in highly ordered samples, so it is very commonly used for crystalline sample analysis [70].
Constructive interference happens when the scattered rays are in the same phase, which is described by Bragg's law:

$$n\lambda = 2d\sin\theta \quad (1)$$

where n is an integer, $\lambda$ is the wavelength of the radiation, d is the distance between crystal planes and $\theta$ is the diffraction angle [70].

For typical XRD, $\theta$ is rather large, which allows the radiation to interact with the material at deeper levels. However, the conventional XRD is not suitable for thin film analysis due to

mostly going through the film and producing interference from the substrate. To diminish the interference from the substrate, very small diffraction angles (commonly under 3°) can be used that allow the radiation to graze the surface or a very thin layer of the material. That way, the radiation interacts with the material's upper layers, providing information mostly about the thin film and surface structure [71]. For that reason, GIXRD was used in this work to analyse the crystal structure, crystallinity and phase composition of the thin films.

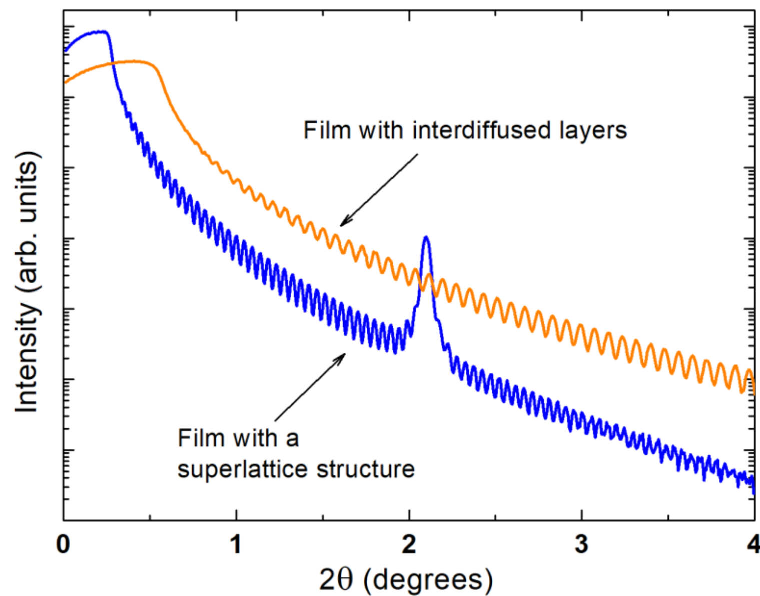


**Figure 3**. XRR patterns of films deposited at $T_G$ = 300 °C with (orange) interdiffused layers and ALD cycle composition of 1 cycle of $GaI_3$-$O_3$ per 1 cycle of $SnI_4$-$O_3$ and (blue) a superlattice structure with ALD cycle composition of 10 cycles of $GaI_3$-$O_3$ per 1 cycle of $SnI_4$-$O_3$.

XRR is a non-destructive method used for the analysis of density, thickness and roughness of single and multilayer thin films [72]. The principles of XRR are similar to GIXRD – the incident radiation is focused onto the sample at very low angles, which after interacting with the material either reflects from the surface or individual interfaces in the material. The interference of those partially reflected x-rays creates a characteristic reflectometry pattern [73] (See Fig 3). The pattern consists of oscillations that give information about the thickness and roughness. Density can be calculated from the first drop of the profile, known as the critical angle [72]. XRR analysis can also detect the existence of superlattice structures, as they can show characteristic diffraction peaks that form when the radiation reflects from layers with different densities. The periodicity of the peaks corresponds to the total thickness of the repeating unit of the superlattice [74].

### *2.3.4 Optical Parameters*

The optical properties of thin films can be characterized by various methods, for instance SE [12], Photoluminescence Excitation Spectroscopy (PLE) [75], and Spectrophotometry [76, 77]. Spectroscopic ellipsometry is a non-destructive optical technique that is based on measuring the change in the polarization state of light when it is reflected from the surface or interfaces of a thin film. The change of polarization depends on the thickness, refractive index and extinction coefficient of the material. By knowing the difference of polarization of incident and reflected light, the former parameters can be determined [78]. A more detailed description of SE can be found at [79].

### *2.3.5 Electrical Properties*

The resistance of thin films can be measured with contact methods, such as 2-point probe and 4-point probe methods, but also with non-contact methods, for instance, Microwave Resonator and Terahertz Time-Domain Spectroscopy (THz TDS) [80]. In this work, a probe station was used to measure voltage as a function of distance between electrodes, which was used to calculate the resistivity.

The 4-point probe method is commonly used to measure the resistance of thin films. In this case, the electricity is intended to travel along the film (surface) rather than pass through the object. The advantage of the 4-point probe method is that it eliminates the contact and wire resistances from the measurements [81].

In this thesis, the resistivity ($\rho$) of the films was calculated from the measured voltage values with the following formulas:

$$R = \frac{\Delta U}{I} \tag{2}$$

where $R$ is resistance, $I$ denotes the applied current and $\Delta U$ is the measured voltage between electrodes.

Resistivity was then calculated as:

$$\rho = R * \frac{A}{l} \tag{3}$$

where $\rho$ is the resistivity of the film, $R$ is the calculated resistance, $A$ denotes the cross-section area under the electrode and $l$ describes the distance between the electrodes.

# 3 EXPERIMENTAL PART

## 3.1 Deposition of $Ga_2O_3$, $SnO_2$ and $Ga_2O_3$-$SnO_2$ Based Thin Films

$Ga_2O_3$, $SnO_2$ and Sn-doped $Ga_2O_3$ thin films were synthesized on Si(100) and $SiO_2$ substrates at growth temperatures ($T_G$) of 150-500 °C using laboratory-made ALD reactor [82]. Si(100) and $SiO_2$ substrates were cleaned before inserting them into the reactor by submerging them into $H_2SO_4$:$H_2O_2$ 5:2 solution at 80 °C for 30 seconds, followed by an ultrasound bath with distilled water for 5 minutes. After the ultrasound bath, Si(100) samples were etched for 30 seconds in 5% HF solution, followed by 2 minutes of ultrasound bath. $Ga_2O_3$ was synthesized using $GaI_3$ (Gallium (III) iodide, anhydrous, 99%, Strem Chemicals, Inc.) and ozone, while $SnO_2$ was grown from $SnI_4$ (Tin (II) iodide, 99%, Strem Chemicals, Inc.) and ozone. $N_2$ (AS Linde Gas, 99.999%) was used as the carrier and purge gas (70 sccm). To obtain sufficient vapour pressure of $GaI_3$ and $SnI_4$, the sources of those precursors were heated up to 150 and 95 °C, respectively, inside the reactor. Oxygen precursor ($O_3$) was generated in a BMT Messtechnik 802N generator from $O_2$ (AS Linde Gas 99.999%). The concentration for $O_3$ during the thin-film deposition was set at approximately 250 $g/m^3$. The ALD cycle time parameters used for the deposition of binary $Ga_2O_3$ and $SnO_2$ films were 5 s of metal precursor pulse, 2 s for the first $N_2$ purge, 2 s for the $O_3$ and 2 s for the second purge. The number of ALD cycles was fixed to 500. The temperatures of the $GaI_3$ and $SnI_4$ sources, process time parameters and $O_3$ flow were chosen from the QCM studies made before the film deposition using a Q-pod quartz crystal monitor (Inficon). For the deposition of doped and mixed films, 1 to 20 $GaI_3$-$O_3$ per 1 to 20 cycles of $SnI_4$-$O_3$ was applied. This kind of supercycle was repeated 17 to 250 times (App. 1). For electrical measurements, titanium-gold electrodes were deposited by electron beam evaporation (EBE) through a stripe shadow mask (Fig. 4) onto samples that were synthesised on $SiO_2$ substrate. The length of the Ti-Au electrodes was set as 6 mm, while the width was 0.2 and 0.1 mm for two outer electrodes and four inner electrodes, respectively. Each electrode was separated with a fixed distance of 0.44 mm. The design of the shadow mask is shown in Fig. 4a and App. 2.

## 3.2 Sample Characterization

The elemental composition of the thin film samples was analysed with an X-ray fluorescence spectrometer ZSX-400 (Rigaku Corp.). The phase composition of the deposited films was examined with a SmartLab X-ray diffractometer (Rigaku Corp.). Measurements were conducted with CuKα radiation generated at a tube power of 8.1 kW and at the incidence angle (ω) of radiation was 0.5° in GIXRD studies. Thickness, surface roughness, and density analysis was done by SmartLab X-ray diffractometer using the X-ray reflectivity mode. The fitting model for doped films was specified as a Si(100) substrate, $SiO_2$ interface layer, a thin layer of $Ga_2O_3$ followed by a layer of $Ga_2O_3$-$SnO_2$, where the content of each compound was defined from the ratio of subcycles (App. 3a). The model for films with SL structures consisted of a Si(100) substrate, a layer of $SiO_2$ and two sets of alternating layers of $Ga_2O_3$ and $SnO_2$, where the middle layers were set to multiply periodically equal to the number of supercycles (App. 3b). A spectroscopic ellipsometer GES-5E (Semilab, Inc.) was used to evaluate the thickness and optical properties of the samples. The angle of incidence was kept at 75° and the wavelength range was 240–900 nm. Refractive index *n*, extinction coefficient *k*, and film thickness values were calculated from the data acquired from SE measurements. The obtained curves were fitted with the Tauc-Lorenz model, where the optical model was defined as a Si(100) substrate and a single layer of the investigated material. The voltage drop measurement values were acquired at Probestation MPS150 (Cascade Microtech) with Keithley 2636A sourcemeter. Electrical measurements were conducted in two different light modes – dark and UV light (265 nm). The UV LED was placed 2 cm above the sample during measurements. Constant current was applied to the furthest electrodes (1 and 6), and voltage was measured across electrodes 1 to 5 (Fig. 4b). The measurement devices were connected to a computer and LABVIEW data system for automatic data recording.

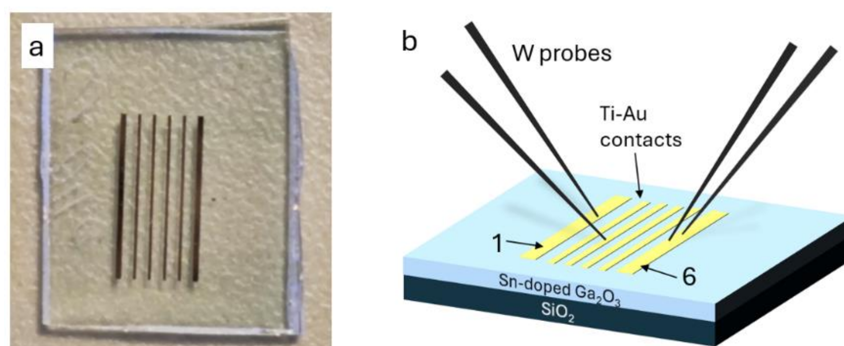


**Figure 4**. (a) Illustration of Ti-Au contacts on deposited films with $SiO_2$ substrate and (b) the scheme of voltage measurement setup with 4 probes.

# 4 RESULTS AND DISCUSSION

## 4.1 Growth of $Ga_2O_3$ and $SnO_2$ Thin Films

Real-time QCM studies were conducted before the growth experiments to characterise the deposition parameters and to optimise the film growth. This kind of study allowed to determine the right cycle times and sublimation temperatures ($T_S$) to ensure the saturation of the growth needed for the self-limiting ALD processes. Figure 5 depicts the QCM patterns of binary $Ga_2O_3$ and $SnO_2$ thin films. For both precursors, the QCM studies were performed at $T_G$ = 150 °C with varying $T_S$. The lowest $T_S$ ensuring the adsorption saturation at acceptable $GaI_3$ and $SnI_4$ pulse duration were 133 °C and 93 °C, respectively. The obtained values for $T_S$ of both precursor combinations were a bit higher compared to previous works done in the same laboratory [19, 63]. However, it is not surprising since a different ALD device with a different deposition configuration was used. In this case, one must consider that previously there have been demonstrated that even the change of the flow rate inside the reactor can influence the growth rate [83], or the length of the pulse duration can influence the film structure [84]. The optimal ALD cycle time parameters 5-2-2-2 s were found suitable for both $GaI_3$-$O_3$ and $SnI_4$-$O_3$ processes.

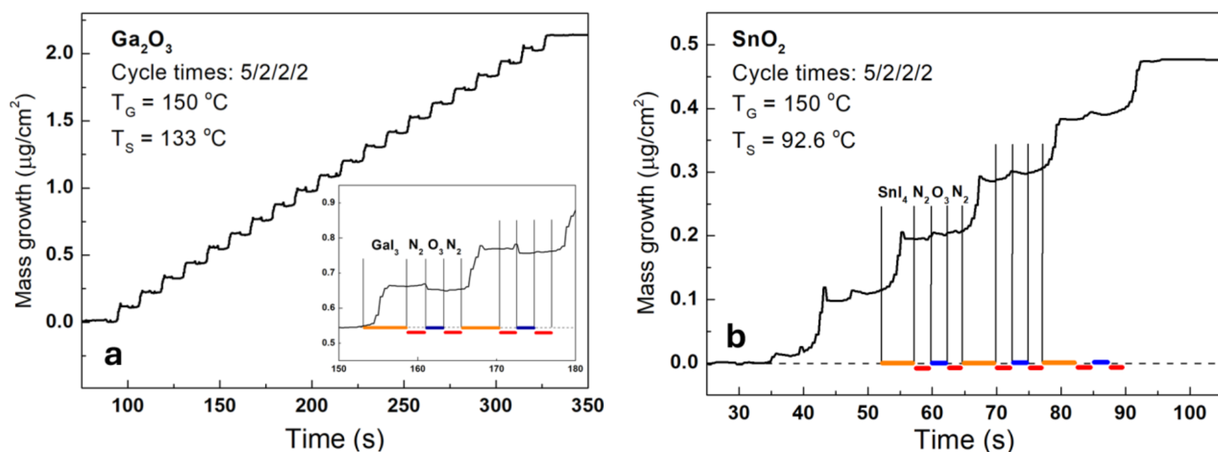


**Figure 5**. QCM signal recorded as a function of time for (a) $GaI_3$-$O_3$ and (b) $SnI_4$-$O_3$ processes. QCM signal has been converted to the mass growth from the XRF measurements.

Elemental composition and the properties of binary gallium and tin oxide films deposited with 500 ALD cycles were investigated to understand how the change of the $T_G$ affects the growth per cycle (GPC). The thickness values were acquired from SE analysis and ranged from 86.9 to 108.1 nm for $Ga_2O_3$ and 88.5 to 136.1 nm for $SnO_2$, respectively. The highest GPC for $Ga_2O_3$

was seen at 200 °C, being 0.216 nm/cycle. It decreased to 0.174 nm/cycle as the $T_G$ increased to 450 °C, reaching a small plateau between 450 and 500 °C (Fig. 6a). The concentration of iodine impurities was the highest in the films deposited at 150 °C, being about 3 at% (Fig. 6b), and was decreasing with increasing $T_G$, reaching the XRF detection limit at $T_G = 400$ °C. In this work, the GPC values measured for deposited $Ga_2O_3$ films were 30–60% higher compared to those presented in a previous work by *Aarik et al* [63], where an especially big difference was seen at $T_G = 500$ °C. However, previous study has demonstrated that from $T_G > 450$ °C, the GPC will be more influenced by different deposition parameters. For instance, the existence of a thickness gradient depending on the sample position in the ALD chamber was seen and the effect increased with increasing $T_G$.

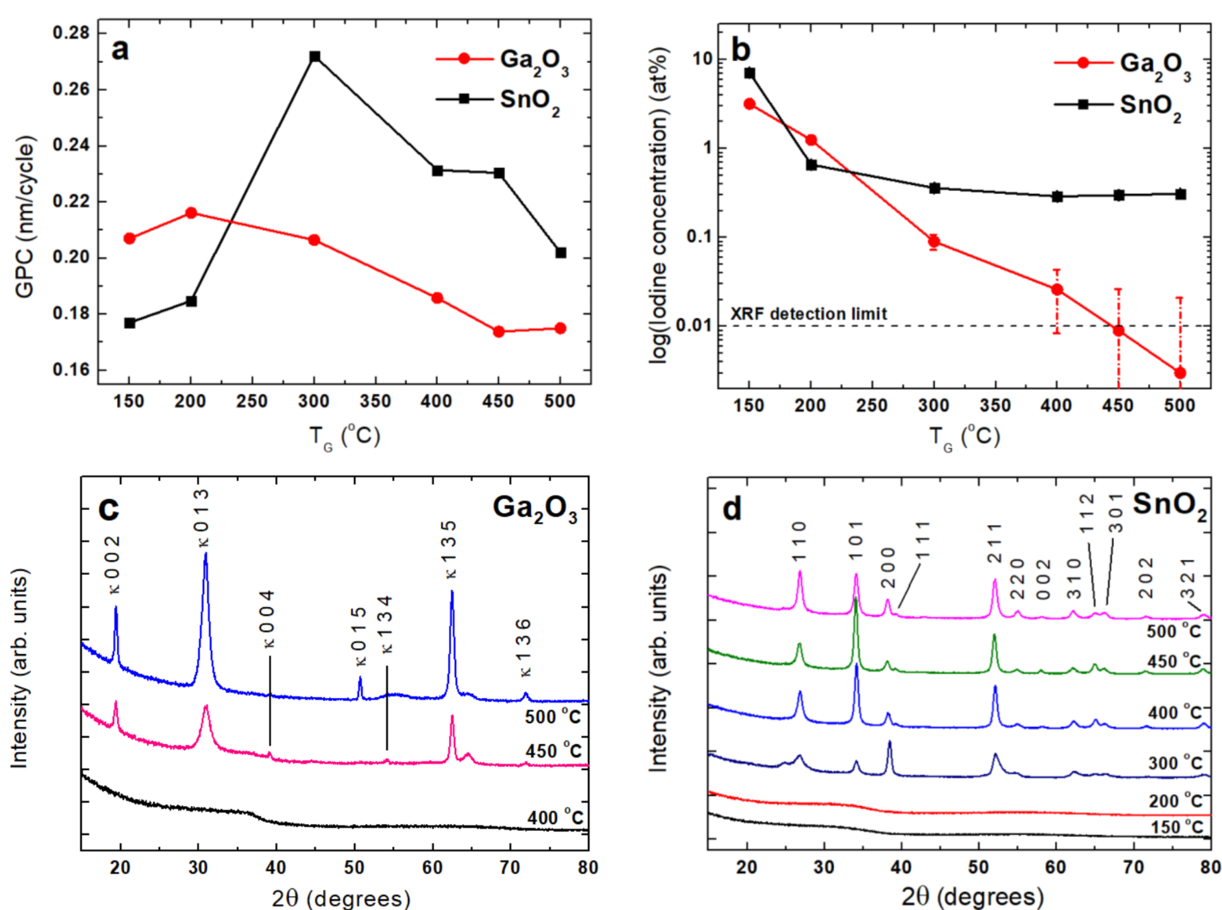


**Figure 6**. (a) The GPC of binary $Ga_2O_3$ and $SnO_2$ films at varying $T_G$, deposited with 500 ALD cycles, (b) Iodine concentration at different $T_G$ in the pure $Ga_2O_3$ and $SnO_2$ films, (c) GIXRD patterns of binary $Ga_2O_3$ and (d) binary $SnO_2$ films at different $T_G$.

The $Ga_2O_3$ films grown at $T_G < 400$ °C were X-ray amorphous (Fig. 6c), whereas ones deposited at $T_G > 450$ °C were starting to crystallize. In the case of the latter ones, it was possible to see reflections peaking at 19.4, 30.9, 38.9, 54.1, 62.5 and 71.9° that could be indexed as 002, 013,

004, 134, 135 and 136 reflections of κ-Ga2O3 [63]. However, as some of the reflections of ε- and κ-$Ga_2O_3$ phases overlap, the presence of either phase could not be excluded. Additionally, broadening of the 134 maximum and the disappearance of 004 reflection could be seen when the $T_G$ was increased from 450 to 500 °C. Furthermore, an additional reflection at 50.6° was observed that could be indexed as 015 of the κ-$Ga_2O_3$ phase, according to *Aarik et al* [63].

On the contrary of the $GaI_4$-$O_3$ process, the GPC of $SnO_2$ films deposited by $SnI_4$-$O_3$ had the lowest GPC value (0.174 nm/cycle) at $T_G$ = 150 °C and reached the maximum value of 0.27 nm/cycle when the $T_G$ was increased to 300 °C (Fig. 6a). When further increasing the $T_G$ to 400 °C, the GPC decreased and stayed on a plateau at about 0.23 nm/cycle up to 450 °C, where it further dropped as the $T_G$ was increased to 500 °C. One of the reasons for the low GPC could be the relatively high impurity concentration in thin films synthesised at $T_G$ = 150 °C, being about 7 at% according to the XRF measurements. Moreover, it needs to be considered that the GPC depends on the concentration of adsorption sites and/or the steric hindrance of the surface compounds, which is related to the amount of large iodide ligands adsorbed together with Sn. Therefore, as the concentration of iodine decreased with the increase of the $T_G$ (reaching a steady concentration of about 0.3–0.4 at% from 300–500 °C), it could have influenced the GPC as well (Fig. 6a-b).

The GIXRD study revealed that the crystallization of $SnO_2$ appeared at $T_G \geq 300$ °C, while the films grown at $T_G < 300$ °C were X-ray amorphous (Fig. 6d). The reflections observed at 26.7, 34.1, 38.4, 52.1, 54.8, 62.2, 64.9, 66.3 and 78.9° could be indexed as 110, 101, 200, 211, 220, 310, 112, 301 and 321, respectively, belonging to tetragonal $SnO_2$ (JPDS No. 01-077-0447). However, an additional reflection was seen at approximately 24.8° that could not be identified. The same maximum has been previously assigned to monoclinic $I_2O_5$ in a work by *Kalam et al* [19], although, the concentration of iodine is too low for that in this work.

An interesting result was the diminution of the intensity of the strongest reflection of the tetragonal $SnO_2$ at 33.7° (101) and the increase of the 37.8° maximum, indexed as 200 that could be seen at $T_G$ = 300 °C. Nevertheless, the ideal powder XRD intensity of the 101 reflection of tetragonal $SnO_2$ should be about 4 times stronger than that of the 200 reflection (JPDS No. 01-077-0447), so one can conclude that it is related to the preferential orientation of crystallites. Furthermore, when increasing the $T_G$ from 400 to 500 °C, additional maxima at 39.2, 58.1 and 71.5° emerged that could be indexed as 111, 002 and 202 for tetragonal $SnO_2$ (JPDS No. 01-077-0447).

## 4.2 Growth and the Phase Composition of $Ga_2O_3$-$SnO_2$ Thin Films

Thin films with different cation ratios were synthesised at $T_G$ = 300 and 450 °C to investigate how the concentration of Ga or Sn affects the growth and film properties. Those $T_G$ were chosen as the XRF and GIXRD (Fig. 6a-c) studies demonstrated different phase compositions in the binary $Ga_2O_3$ and $SnO_2$ films with comparably low impurity concentrations. From here on, the cycles of $GaI_3$-$O_3$ and $SnI_4$-$O_3$ are denoted as G and S, respectively.

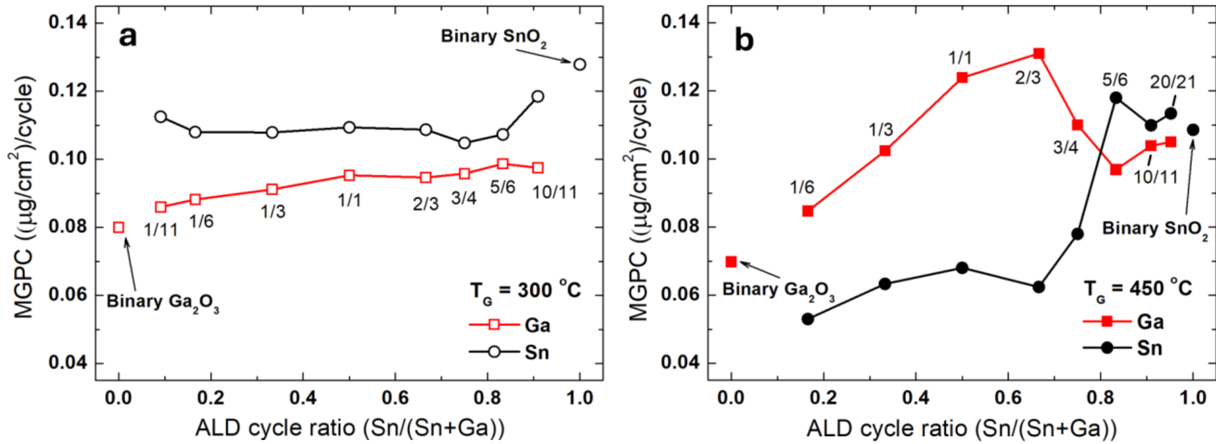


**Figure 7**. (a) and (b) Sn-doped $Ga_2O_3$ thin films MGPC as a function of ALD cycle ratios and $T_G$. The ALD cycle ratios are denoted as the fraction of S cycles to the sum of S and G cycles.

The XRF study made for GTO films and heterostructures demonstrated that MGPC determined for Ga and Sn was remarkably dependent on the S/(S+G) ALD cycle ratio. For the films deposited at $T_G$ = 300 °C, the highest MGPC (0.099 µg/cm$^2$ per cycle) was determined for Ga when the S/(S+G) ALD cycle ratio was 5/6 (Fig. 7a). Furthermore, when the number of sequential G cycles increased from 1 to 10 after an S cycle (Fig. 7a, S/(S+G) ALD cycle ratio 1/1 to 1/11), the Ga MGPC decreased from 0.095 to 0.085 µg/cm$^2$ per cycle. However, it was possible to see that when the number of the S cycles made before G cycles increased from 1 to 10, the MGPC for Ga did not change significantly (Fig. 7a, S/(S+G) ALD cycle ratio 1/1 to 10/11), where it stayed between 0.095 and 0.097 µg/cm$^2$ per cycle, respectively.

On the other hand, the MGPC for Sn was the highest in binary $SnO_2$, about 0.13 µg/cm$^2$ per cycle. The mass growth rate decreased as 1 cycle of G was added after every 10 cycles of S, to 0.12 µg/cm$^2$ per cycle. Interestingly, almost no change in the MGPC of Sn was detected when 1 to 5 ALD cycles of S were deposited after 1 G cycle (Fig 7a, S/(S+G) cycle ratio 1/1 to 5/6), where the values remained between 0.109 and 0.107 µg/cm$^2$ per cycle. However, the increasing

thickness of the $Ga_2O_3$ layer and ALD cycles of G made from 5 to 10 caused the increase in $SnO_2$ growth rate from 0.108 to 0.113 μg/cm$^2$ per cycle.

Similarly to 300 °C, the MGPC of Ga was the lowest in the case of binary $Ga_2O_3$ films deposited at $T_G$ = 450 °C (Fig. 7b) and with the decreasing number of G cycles from 5 to 1, it increased from 0.085 to 1.13 μg/cm$^2$ per cycle, respectively. Compared to the films deposited at 300 °C, the increase of the S cycles made before G cycles had a remarkable effect – by increasing the number of S cycles from 2 to 5, the MGPC of Ga already started to decrease and reached the value of 0.097 μg/cm$^2$ per cycle when 5 cycles of S have been deposited before 1 cycle of G (Fig. 7b). Surprisingly, the growth rate of Sn increased when 1 cycle of G was deposited between 2 to 20 cycles of S, from 0.062 to 0.113 μg/cm$^2$ per cycle, respectively (Fig. 7b). However, it could be seen that the growth rate decreased with increasing number of G cycles from 1 to 5 between 1 cycle of S, to 0.05 μg/cm$^2$ per cycle.

From these results, one can conclude that at both $T_G$, there are more effective nucleation sites for gallium oxide when the surface is covered with a layer of at least 1 cycle of S. A similar behaviour has been observed previously in a work by *Aarik et al* [85] of $Al_2O_3$, deposited using $AlCl_3$ and $O_3$, where more than 3 times higher growth rate values were obtained at the surface of $TiO_2$ than $Al_2O_3$. In this instance, one could argue that the differences in diffusion of two oxides and oxygen concentration on the surface or the reaction of one metallic precursor and another oxide, causing the formation of volatile compounds that are removed from the surface during the metallic precursor pulse, could be considered as logical explanations.

GIXRD was performed to analyse the influence of film composition and $T_G$ on the structure of the GTO thin films. Based on those studies, the intensity of the reflections emerging at 38.5 and 52.2° that could be indexed as 200 and 211, belonging to rutile $SnO_2$, started to diminish when gallium oxide was introduced to the structure. At the same time, broadening of less intense reflections could be noticed for the films deposited at $T_G$ = 300 °C (Fig. 8a). Furthermore, a slight shift of about 0.2 degrees to the higher angle could be seen in the reflection positions, which may be explained by the smaller ionic radius of $Ga^{3+}$ compared to $Sn^{4+}$, according to *Mi et al* [37]. Hence, the lattice plane distance decreased as gallium replaced $Sn^{4+}$ atoms, resulting in a shift of the reflection position as demonstrated in Fig. 8a. The films became X-ray amorphous when the ratio of Sn to Ga was about 4 to 1 and remained non-crystalline until binary $Ga_2O_3$, which could be explained by the low $T_G$ of $Ga_2O_3$ (Fig. 6c). Additionally, at

small doping concentrations, the Ga atoms might incorporate into the $SnO_2$ lattice by substituting Sn atoms or by occupying Sn vacancies [86] without distracting the structure of $SnO_2$. However, higher concentrations may lead to the formation of large, non-crystalline Ga-dense layers that render the films amorphous.

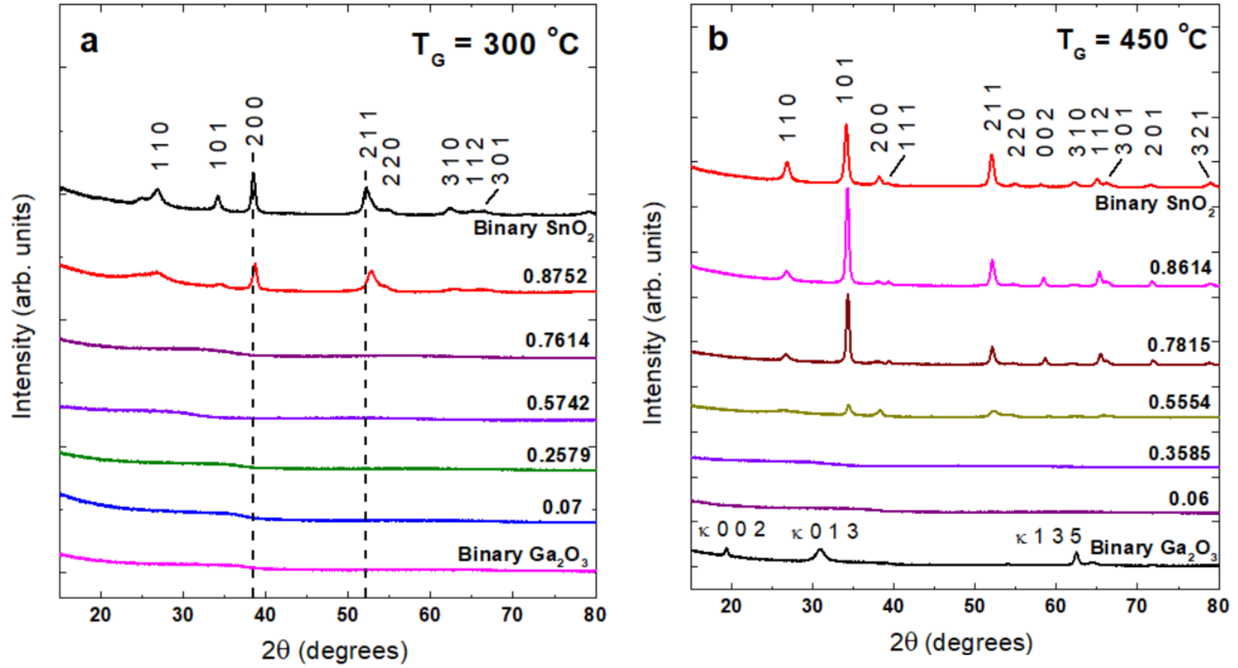


**Figure 8**. GIXRD diffraction patterns of Sn-doped $Ga_2O_3$ films with varying cation ratios, synthesised at (a) $T_G$ = 300 °C and (b) $T_G$ = 450 °C. The Sn/(Sn+Ga) ratios are marked on the right side of the graphs. The indices depicted on the graph (a) belong to the tetragonal $SnO_2$ and those presented on the graph (b) belong to the tetragonal $SnO_2$ (upper side) and κ/ε-$Ga_2O_3$ (lower side).

At $T_G$ = 450 °C, the diffraction pattern of binary $Ga_2O_3$ film showed the existence of crystalline phases, evident in the reflections that emerged at 19.3, 30.9 and 62.4° that could be indexed as 002, 013 and 135, belonging to κ/ε-$Ga_2O_3$ (Fig. 8b). Remarkably, the GIXRD reflections of κ/ε-$Ga_2O_3$ disappeared already when 1 cycle of S had been added after 5 cycles of G. This could indicate that the κ/ε-$Ga_2O_3$ phases already destabilised when a small amount of foreign atoms was introduced to the structure as stated by *Mi et al* [37]. Notably, it was possible to observe traces of the peaks belonging to $SnO_2$ when the cycle ratio used in ALD was 1 to 3 and the cation ratio, according to XRF, was 0.55. Furthermore, the intensity of 101 reflection did not decrease as much as the reflection of 211 with the increase of Ga concentration in the films from 0.14 to 0.22. This could indicate that while doping the $SnO_2$ films with gallium oxide, the preferable orientation on 101 of tetragonal $SnO_2$ could be stabilised.

The correlation of the changes in the film structure and MGPC can be seen when analysing the results of the GIXRD and XRF (Figs. 7a-b and 8a-b). At both $T_G$'s, the MGPC of Sn decreased as the films became X-ray amorphous, indicating that the amorphous phase grows slower than the crystalline phase.

XRR analysis demonstrated that the thickness, density, and roughness of the synthesised films depended on the composition of the ALD cycle. The density of the GTO films and heterostructures consistently increased as the number of G cycles decreased and S cycles grew, increasing from 5.6 g/cm$^3$ for 20G + 1S to 7.2 g/cm$^3$ for 1G + 10S, respectively (Table 1). Notably, the roughness values remained in sub-nanometre range for films with 1 to 20 cycles of G per 1 cycle of S. However, as the number of S cycles increased from 2 to 10 per 1 cycle of G, the films started to display higher roughness, reaching the highest value of 4.8 nm for 1 to 2 cycles of G and S, respectively. Additionally, it was seen that the films' thicknesses increased from 110 nm for 20G + 1S to 123 nm for 1G + 5S as the amount of S cycles grew in the ALD cycle composition.

**Table 1.** Thickness, density and roughness of deposited films at $T_G$ = 300 °C, analysed with XRR.

| Cycle composition | Thickness (nm) | Density (g/cm$^3$) | Roughness (nm) |
|---|---|---|---|
| 20G + 1S | 110 | 5.6 | 0.4 |
| 5G + 1S | 112 | 5.7 | 0.5 |
| 1G + 1S | 122.5 | 6.22 | 0.5 |
| 1G + 2S | 121 | 6.4 | 4.8 |
| 1G + 5S | 123 | 6.8 | 0.7 |
| 1G + 10S | 118.3 | 7.2 | 4 |

The higher surface roughness for films with a larger S cycle ratio compared to those with a higher number of G cycles could be explained by the crystallinity of the films, as those were seen to exhibit crystalline phases belonging to $SnO_2$ (Fig. 8a). As such, one could argue that the amorphous state allowed films to grow more uniformly, while the crystalline structure increased grain boundaries and lattice defects, inducing surface non-uniformities and thus increasing the roughness of the films.

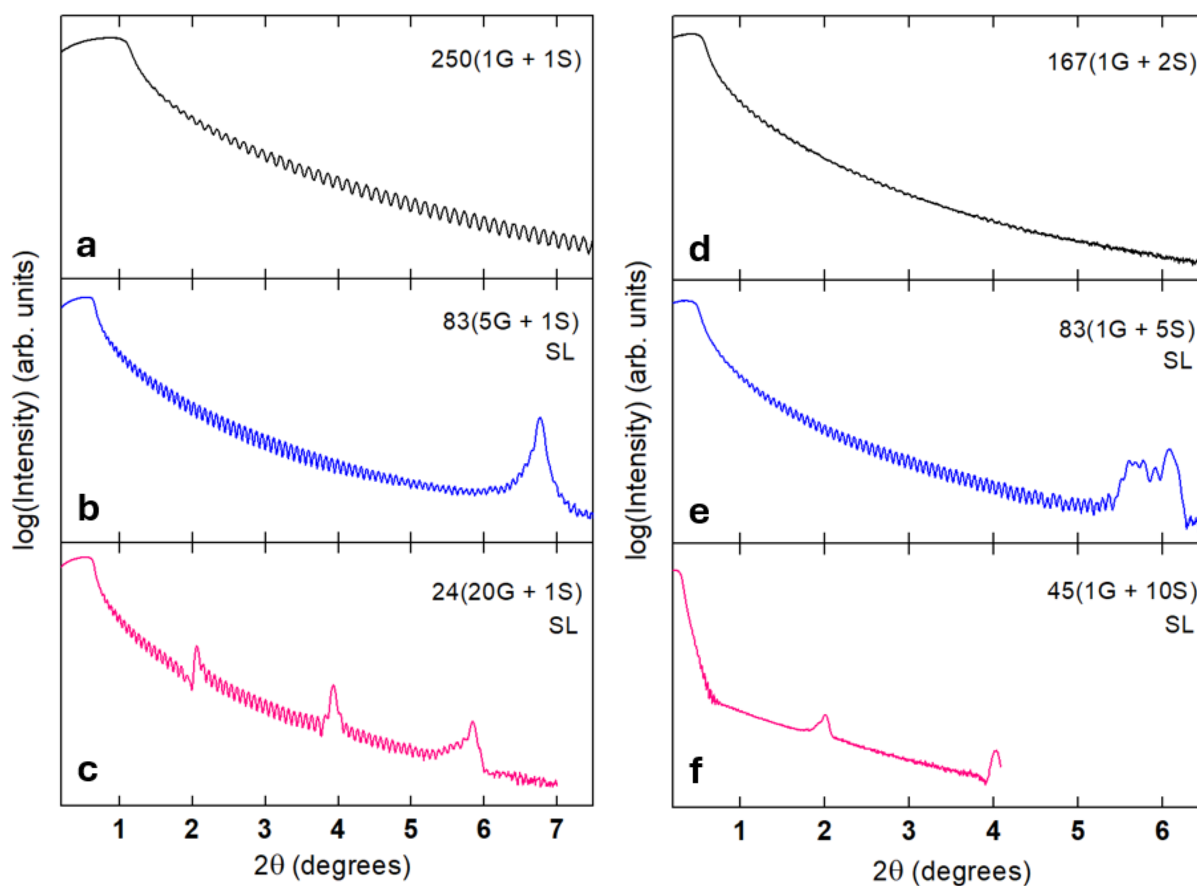


**Figure 9**. XRR patterns of thin films synthesised at 300 °C with varying G-S cycle ratios and cycle repetitions. G and S represent the cycles of $GaI_3$-$O_3$ and $SnI_4$-$O_3$, respectively. The films exhibiting superlattice structures are marked as SL.

Additionally, as an interesting result, the XRR measurements helped to understand how the layers of gallium oxide and tin oxide were positioned in the GTO heterostructures. The XRR pattern of thin film with a 1-1 ratio of G and S cycles showed clear and periodic oscillations (Fig. 9a) with no diffraction peaks, which suggested that for the smallest G-S cycle ratio, the deposited layers became intermixed. However, as the number of G or S cycles increased (5-1 or 1-5), the films started to develop diffraction peaks that became more frequent as the cycle ratio rose (Figs. 9b, c, e and f). The periodicity of the diffraction peaks gives insight into the thickness of one bilayer in the superlattice, so one might conclude that the diffraction maxima were present more frequently in XRR plots of films with thicker bilayers. A similar behaviour was seen in a previous study by *Yu et al* [87], where the diffraction peaks reoccurred more often as the thickness of layers in the superlattice films was increased.

The XRR patterns acquired from films with $T_G$ = 450 °C started to show signs of a superlattice structure from cycle ratios of 2-1 and 1-10 for G and S, respectively. Distinct diffraction peaks

were not seen for films with thinner layers, meaning that the $T_G$ was high enough to allow the layers to diffuse together. The phenomenon was also noticed in a work by *Yu et al* [87], where as-deposited films exhibited superlattice structures that disappeared when they were annealed at >400 °C.

The data obtained from XRF analysis demonstrated that the concentration of iodine for films synthesised at 300 and 450 °C exhibited similar increasing behaviour with the increase of Sn content in the films (Fig. 10). Furthermore, the concentration of iodine in films deposited at $T_G$ = 450 °C was constantly lower compared to those grown at 300 °C and reached the XRF detection limit at a very low Sn content. The highest iodine concentration values for films deposited at 300 and 450 °C were 0.3 and 0.27 at%, respectively.

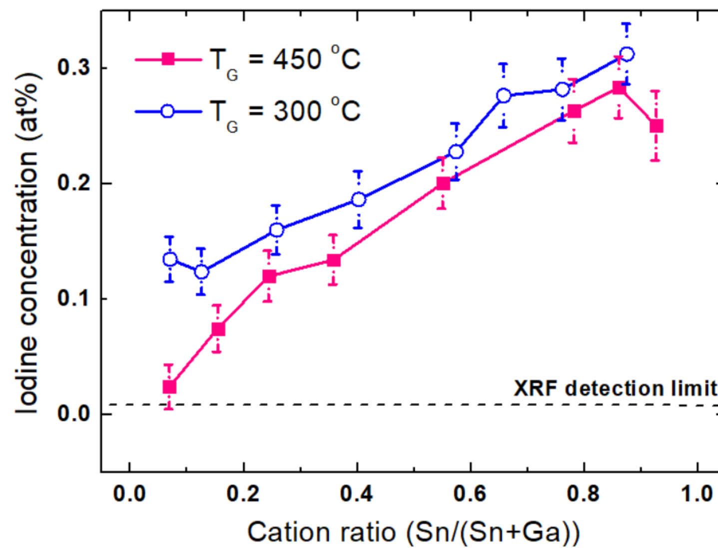


**Figure 10**. Iodine concentration as a function of $T_G$ and cation ratio.

## 4.3 Optical Properties

Spectroscopic ellipsometry analysis was conducted to understand if the $T_G$ and doping concentration had any influence on the refractive index (*n*) and extinction coefficient (*k*) values of the deposited thin films. The *n* that was determined at the wavelength of 633 nm increased linearly from 1.89 to 2.04 with the increase of the cation ratio from 0.07 to 0.76 for films deposited at $T_G$ = 300 °C (Fig. 11). The obtained refractive indices were higher compared to

binary $Ga_2O_3$ film synthesised at the same $T_G$, demonstrating an $n$ value of 1.88 at 633 nm (Fig. 11). Notably, it was seen that the $n$ values between Sn/(Sn+Ga) ratio of 0.76 to 1 remained almost constant and about the same as that of binary $SnO_2$, showing an $n$ value of approximately 2.05. This behaviour could be explained by the information about the structure of $Ga_2O_3$-$SnO_2$ thin films obtained from GIXRD analysis, where the onset of crystalline $SnO_2$ phase formation was observed to start between cation ratios of 0.76 and 0.87 (Fig. 8a). As the crystalline phase is denser compared to the amorphous state, the refractive index increased. The lowest and highest $n$ values are comparable with refractive indices of binary $Ga_2O_3$ and $SnO_2$, respectively, as stated in previous studies [19] [20] [24].

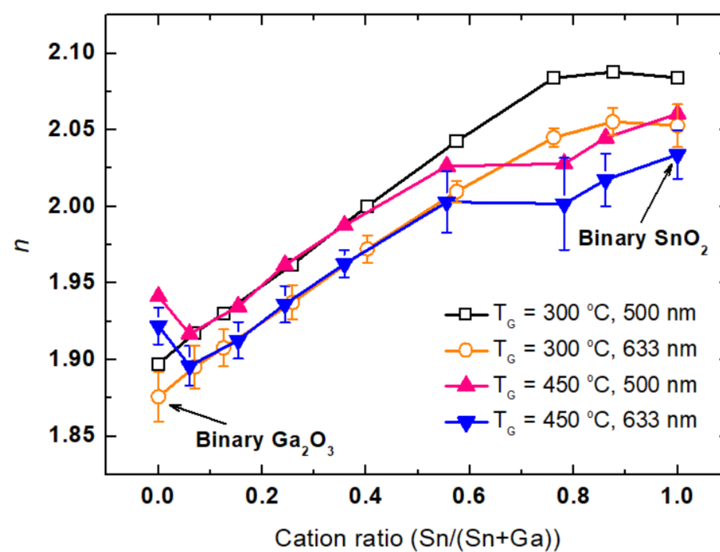


**Figure 11**. Refractive index as a function of cation ratio of thin films grown at 300 °C and 450 °C, measured at 500 and 633 nm wavelength by spectroscopic ellipsometry. Error bars are shown for measurements at 633 nm wavelength.

Compared to the behaviour of the refractive index seen for films deposited at $T_G$ = 300 °C, the lowest $n$ value (about 1.89) was seen when the film was deposited using ALD cycle composition of 5G+1S and with a cation ratio of 0.06 at $T_G$ = 450 °C (Fig. 11). A similar increase in $n$ values was observed for films with a Sn/(Sn+Ga) ratio of 0.06 to 0.55. However, slight differences occurred in the refractive index from ratios >0.55, where the $n$ was seen to remain at approximately 2.0 and slightly increased to the highest value of 2.03 for binary $SnO_2$.

Interestingly, two phenomena can be seen for films deposited at 450 °C – the initial higher $n$ of binary $Ga_2O_3$ and the slight kink in the refractive index at 0.78 Sn/(Sn+Ga) ratio. The former could be explained by the crystallinity of $Ga_2O_3$ at 450 °C (Fig. 8b), as the crystalline phase has higher density and long-range ordering that can enhance the interaction of light with the

material [88], which consequently shows in higher *n* values. When Sn is incorporated into the material, the long-range ordering might deteriorate and thus, the refractive index might decrease. A decreasing behaviour of the *n* value at relatively low doping concentrations was also demonstrated in an earlier study by *Shen et al* [28]. As the $Ga_2O_3$ films were doped with increasing levels of Sn (up to 20%), the diminution of *n* was seen and was thought to arise due to the increase in the concentration of free carriers with the growth of Sn content in the films. At higher doping levels (50%), an increase in refractive index value was observed.

The slight kink of *n* at 0.78 Sn content might be explained by the S to G cycle ratio in the ALD cycle composition (Fig. 7b) and film crystallinity at $T_G$ = 450 °C (Fig. 8b). It was seen that the growth rate of Sn increased when the number of S cycles was larger than 1 per 1 cycle of G. Furthermore, crystalline phases belonging to $SnO_2$ were detected for films with Sn/(Sn+Ga) ratio >0.55 and with G-S cycle ratio of 1 to 3. Hence, from a certain cycle ratio, the growth rate of crystalline $SnO_2$ with high roughness was enhanced and thus, the value of *n* decreased. Additionally, another explanation might be that the optical model used for fitting the data obtained from SE analysis did not satisfy the conditions for fitting the optical properties very well and consequently, the fitted values might have higher uncertainties (Fig. 11).

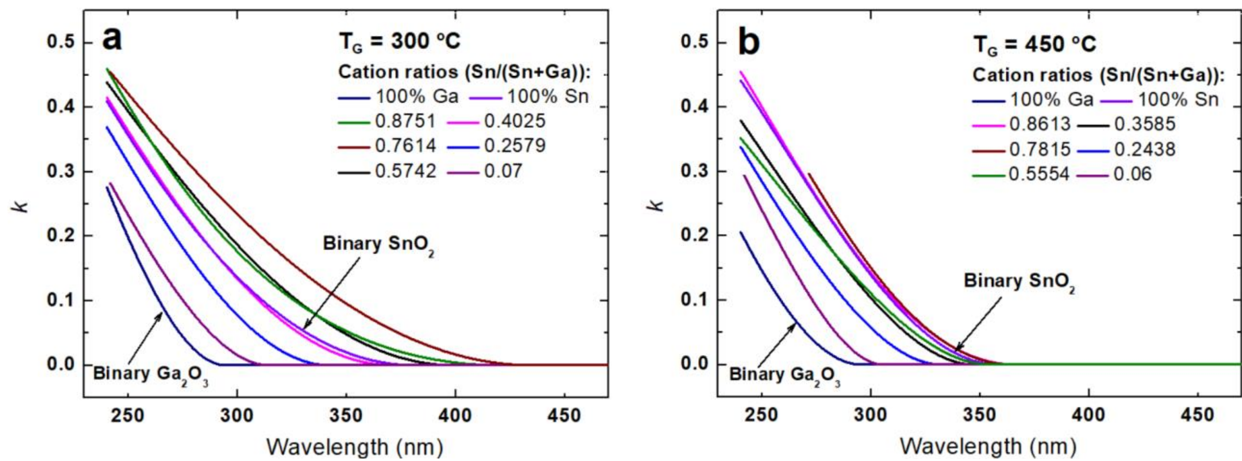


**Figure 12**. Extinction coefficient as a function of wavelength of thin films grown at (a) 300 °C and (b) 450 °C with varying cation ratios.

The values of *k* for films synthesised at 300 °C demonstrated an increasing behaviour from binary $Ga_2O_3$ to a film with 25% Sn content. However, the films with a cation ratio >0.25 exhibited higher *k* values than that of $SnO_2$. One possible explanation may be the high surface roughness of Sn-rich films (Table 1), causing light scattering which decreases the film reflectivity and increases the extinction coefficient. This is also in agreement with an earlier

study by *Shen et al* [28], where Sn-rich films demonstrated high roughness and $k$ values. This phenomenon could also be the result of the formation of an impurity-like band into the $Ga_2O_3$ when doping it with Sn. Previously, a study by *Mehr et al* [89] demonstrated similar behaviour with CrTiO films, where a slight increase in absorbance and reduction of $E_g$ were observed when chromium oxide was doped with titanium.

Films grown at $T_G$ = 450 °C showed similar trends in the $k$ values to those synthesised at 300 °C, with the lowest extinction coefficient observed for binary $Ga_2O_3$. As the Sn content increased over 0.78, the $k$ values became comparable to or slightly higher than binary $SnO_2$. Close to 0 values of $k$ are noticeable at 350 nm, a slightly shorter wavelength compared to those grown at 300 °C.

## 4.4 Electrical Properties

The probe station was used to measure the voltage as a function of the distance between electrodes in dark and UV light (265 nm) to comprehend how the composition and structure influence the surface resistivity of the films. The resistivities were calculated using the formulas (2) and (3) described previously in chapter 2.3.5.

Figure 13 shows the resistivity of GTO thin films as a function of the cation ratio for samples with different $T_G$ using two different illumination settings. The lowest $\rho$ value, based on the measurements in the dark, was calculated from a sample with 0.66 Sn/(Sn+Ga) ratio, being approximately 0.007 Ω×m for films grown at $T_G$ = 300 °C. Notably, the $\rho$ values were not hugely influenced by the increase of Sn content and only slightly increased until binary $SnO_2$, where $\rho$ of 0.03 Ω×m was obtained. However, a significant rise of $\rho$ values was observed when the level of Ga increased from 0.34 to 0.53, reaching the highest $\rho$ of 11 Ω×m from where on, the voltages were almost impossible to determine with the used measurement configuration. In those cases, the applied currents were remarkably small (in nanoamperes), and a voltage change across electrodes was not detected. Thus, the values were considered unreliable. Nevertheless, turning on the UV-light during the measurements increased the conductivity of the thin films and made it possible to gather reliable data from films having Sn/(Sn+Ga) ratios <0.47 (Fig. 13). Compared to the last valid measurement in the dark with a calculated $\rho$ of 11 Ω×m, using UV-light increased the conductivity of the same film and lowered the $\rho$ to 0.3 Ω×m. However,

the resistivity values rose in a similar fashion when the content of Ga increased to 0.75, showing the highest value of 350 Ω×m. The lowest $\rho$ (0.007 Ω×m) was also observed at 0.66 cation ratio and stayed in the same range as those measured in the dark when the level of Sn increased. Yet, a slight increase in conductivity could be seen for binary $SnO_2$ with the calculated $\rho$ of 0.2 Ω×m.

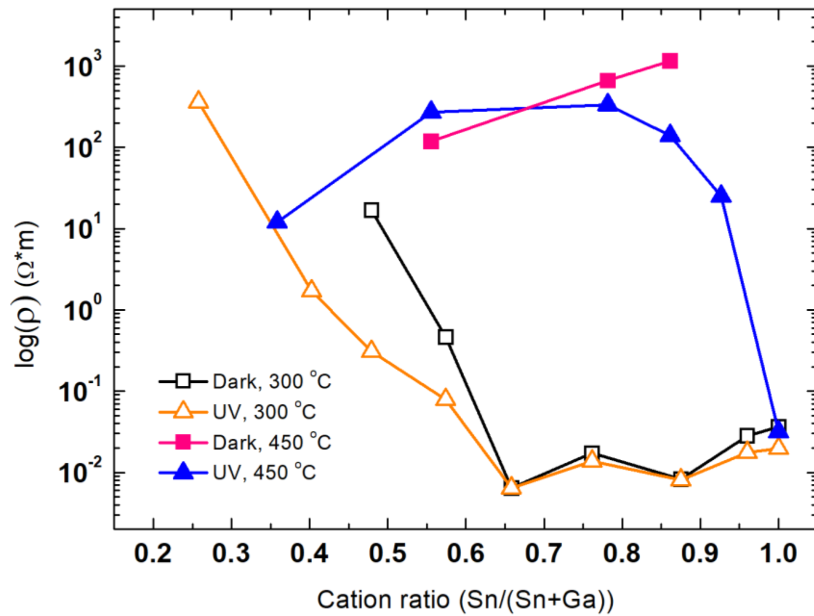


**Figure 13**. Resistivity of the deposited thin films as a function of cation ratio, $T_G$ and illumination mode.

The films synthesised at $T_G$ = 450 °C showed notably different resistivity values compared to those deposited at a lower temperature. The measurements conducted in the dark gave first valid $\rho$ values from Sn content of 0.57 with $\rho$ of approximately 100 Ω×m from where gradual increase could be observed until 1000 Ω×m for 87% Sn film. Additionally, using the UV light allowed to measure voltage changes for a film with an even lower cation ratio (0.35), having $\rho$ of about 10 Ω×m. That is, however, not a surprise as the conductivity of $Ga_2O_3$ can be influenced by UV light and it has been previously shown to be suitable to use in UV-detectors. An increase of resistivity could be seen until 55% of Sn (250 Ω×m), where it stayed on a plateau and plummeted down to 0.03 Ω×m for binary $SnO_2$.

Interestingly, crystallinity has a significant influence on electrical properties. A previous study done by *Miglio et al* [90] has stated that for tetragonal $SnO_2$, the smaller distance between Sn atoms along the c-axis gives a shorter pathway for electrons to move. So, one could argue that the change in the preferred orientation of the crystallites at different $T_G$ (Fig. 8a-b) could be one of the reasons why the resistivity values of the films deposited at 300 and 450 °C differ

remarkably. Another aspect that could influence the electrical properties is the concentration of impurities in the films. Nevertheless, it was seen (Fig. 10) that the highest concentration of iodine reached only 0.3 at% for films with $T_G$ = 300 °C, while those with higher $T_G$ showed even smaller concentrations. Hence, the content of impurities might not have a significant effect on the resistivities in this work.

Moreover, the formation of Ti-Au contacts could possibly affect the calculated resistivities quite a lot. The fabrication of ohmic contacts is crucial for the performance of semiconductor devices as it increases the voltage across the channel and reduces heat generation [91]. In this work, however, one might argue that the interface between the film and titanium formed an additional barrier, which influenced the measurement results. Hence, the measured resistivities could appear much higher due to contact resistance (App. 4). Nevertheless, in an earlier work by *Huan et al* [91], it was stated that high doping could enhance the formation of ohmic contacts, where the energy barrier between metal and semiconductor becomes narrow and allows for electrons to tunnel through the interface. Another way to overcome this problem is to anneal the electrodes, which causes the diffusion of Ti into the surface layer and the formation of $TiO_x$ under the electrodes to help form an ohmic behaviour [92]. This would be the next step in future studies to understand if annealing will help to reduce the rectifying behaviour of the electrodes on Sn-doped κ/ε-$Ga_2O_3$ films.

# SUMMARY

In this thesis, the growth, structural, optical, and electrical properties of atomic layer deposited binary $Ga_2O_3$, $SnO_2$ and $Ga_2O_3$-$SnO_2$ thin films were studied. This work demonstrated that $GaI_3$-$O_3$ and $SnI_4$-$O_3$ could be applied as the precursors for ALD processes and they enabled the synthesis of thin films with low iodine impurity concentrations. Furthermore, the growth rates of gallium and tin oxides depended on the surface, while in the mixed films, the corresponding values were higher in case of $GaI_3$-$O_3$ and similar or lower in case of $SnI_4$-$O_3$ than in binary films. Notably, a decrease in growth rate of $SnI_4$-$O_3$ was seen in X-ray amorphous films.

The phase composition analysis made by GIXRD showed that most of the $Ga_2O_3$-$SnO_2$ heterostructures deposited at 300 and 450 °C were X-ray amorphous and only in films with tin content higher than 76 and 55%, respectively, was possible to detect tetragonal $SnO_2$. The presence of κ/ε-$Ga_2O_3$ was possible to be seen only in binary films, while the film deposited using $GaI_3$-$O_3$ and $SnI_4$-$O_3$ cycle ratio of 5-1, resulting in cation ratio of 0.06 at 450 °C, was already X-ray amorphous. An interesting result from XRR studied showed that the deposited films formed smooth layered system when more than 5-1 or 1-5 cycles of $GaI_3$-$O_3$ and $SnI_4$-$O_3$ were applied, resulting in a superlattice system.

The optical measurements made by spectroscopic ellipsometry demonstrated that the refractive index of $Ga_2O_3$ and $SnO_2$ thin films deposited at 300 °C did not depend on the concentration of Ga and Sn when there was possible to see tetragonal $SnO_2$ phases. However, a linear dependence between cation ratio and refractive index was seen in amorphous films. The refractive indices of films grown at 450 °C behaved in a similar manner but had some deviations at Sn/(Sn+Ga) ratios of 0.06 and 0.78. The extinction coefficients increased from binary $Ga_2O_3$ and exceeded that of binary $SnO_2$ at both $T_G$'s.

The electrical measurements demonstrated a strong dependence on $T_G$ and composition. The Ga-rich films exhibited high resistivity at both $T_G$'s, while the lowest value (0.007 Ω×m) was observed in films grown at 300 °C with the Sn/(Sn+Ga) ratio of 0.66, being lower than 0.03 Ω×m for binary $SnO_2$ deposited at the same temperature. Films grown at 450 °C showed a linear rise in resistivity from 100 to 1000 Ω×m as the content of Sn increased, while using UV light enhanced the conductivity and reduced the resistivity to 10-250 Ω×m across increasing Sn concentration.

Although, as in this thesis, it was possible to deposit films with smooth and uniformly positioned layers, a homogenous diffusion of Sn dopant in $Ga_2O_3$ at concentrations $\leq 3$ at% across the as-deposited films was not achieved. Therefore, further studies are needed in the future.

In conclusion, the findings demonstrate the prospect of $Ga_2O_3$ and $SnO_2$ mixing for tailoring the properties of thin films and that the electrical conductivity and optical characteristics can be improved by optimising the growth conditions and composition. Additionally, the thin films and heterostructures developed in this thesis could be potentially applied in transparent electronics, UV-absorbers in multi-junction solar cells and UV-detectors.

# SUMMARY IN ESTONIAN

Selles magistritöös uuriti aatomkihtsadestusmeetodiga valmistatud $Ga_2O_3$, $SnO_2$ ja $Ga_2O_3$-$SnO_2$ õhukeste kilede kasvu, koostist ja struktuuri ning nende mõju optilistele ja elektrilistele omadustele. Kilede sadestamiseks kasutati metallide lähteainetena $GaI_3$ and $SnI_4$ ning hapniku lähteainena osooni, mis võimaldasid sadestada peaaegu lisanditevabu kilesid. Puhta gallium- ja tinaoksiidi kasvukiirused sõltusid kasvupinnast, seejuures oli märgata, et segukiledes oli võrreldes puhaste materjalidega galliumi kasvukiirus suurem ning tina puhul sarnane või väiksem. Lisaks oli näha, et tina kasuvkiirus vähenes amorfsetes kiledes.

Faasi- ja struktuuriuuringud näitasid, et enamik 300 ja 450 °C juures sadestatud kiledest olid amorfsed, kusjuures oli märgata tetragonaalse $SnO_2$ faase, kui tina sisaldus kiledes oli vastavalt üle 76 ja 55%. κ/ε-$Ga_2O_3$ esinemist nähti ainult puhastes materjalides, samas 450 °C juures sünteesitud kile, mille tina kogus oli 6% ning $GaI_3$-$O_3$ ja $SnI_4$-$O_3$ tsüklisuhe oli 5-1, muutus juba amorfseks. Huvitava tulemusena nähti, et sadestatud kiled moodustasid siledate kihtidega superstruktuure, kui sünteesiprotsessi käigus kasutati rohkem kui 5 tsüklit $GaI_3$-$O_3$ ühe tsükli $SnI_4$-$O_3$ jaoks või vastupidi.

Optiliste mõõtmiste tulemused näitasid, et 300 °C juures sünteesitud $Ga_2O_3$-$SnO_2$ õhukeste kilede murdumisnäitaja ei sõltunud kilede koostisest, kui nendes esines $SnO_2$ kristallfaase. Küll aga märgati lineaarset sõltuvust katioonide suhte ja murdumisnäitaja vahel, kui kiled olid amorfsed. 450 °C juures sadestatud kilede murdumisnäitajad käitusid sarnaselt, kuid mõningad erinevused esinesid 0.06 ja 0.78 katioonide suhete puhul. Mõlematel kasvutemperatuuridel suurenesid neeldumistegurid puhtast galliumoksiidist ning ületasid puhta tinaoksiidi neeldumisteguri väärtuseid.

Õhukeste kilede elektrilised omadused sõltusid kasvutemperatuurist ja kilede koostisest. Mõlemal kasvutemperatuuril olid suure galliumi sisaldusega kiled kõrgete eritakistustega. Kusjuures, madalaimat eritakistust (0.007 Ω×m) täheldati 300 °C juures kasvatatud kilel, mille katioonsuhe oli 0.66 ning oli madalam võrreldes samal temperatuuril sadestatud puhta $SnO_2$ eritakistusega (0.03 Ω×m). Kõrgemal temperatuuril kasvatatud kilede eritakistus tõusis 100 kuni 1000 Ω×m, kuid kilede elektrijuhtivus parenes, kui mõõtmistel kasutati UV-valgust ning vähendas eritakistuse väärtuseid 10 kuni 250 Ω×m-ni.

Selles töös oli võimalik sadestada siledate ja ühtlaselt asetsevate kihtidega struktuure, kuid tina aatomite homogeenset difusiooni galliumoksiidis ≤ 3 at% üle kogu kile ei saavutatud. Seetõttu on tulevikus vaja täiendavaid sadestusparameetrite ja dopeerimise optimeerimise uuringud.

Tulemused näitasid, et $Ga_2O_3$ ja $SnO_2$ segamisel on võimalik muuta kilede omadusi ning elektrijuhtivust ja optilisi omadusi saab parendada optimiseerides kasvutingimusi ja kilede koostist. Lisaks saaks töös arendatud kilesid potentsiaalselt kasutada läbipaistvas elektroonikas, tandempäikeseelementides UV-valgust absorbeeriva kihina või näiteks UV-detektorites.

# ACKNOWLEDGEMENTS

I am thankful to the researchers and professors from the Laboratory of Thin Film Technology for technical assistance, and a special thanks to my fellow students and family for intellectual conversations. I am deeply grateful to my supervisors, Lauri Aarik and Kaupo Kukli, whose guidance and patience helped me throughout the course of this thesis. I could not have asked for better mentors.

The research was funded by the Estonian Research Council (grants PSG448 and PRG2594).

# REFERENCES

[1] A. Rahman, 'A Review on Semiconductors Including Applications and Temperature Effects in Semiconductors', *ASRJETS*, vol. 7, no. 1, 2014, Accessed: May 30, 2025. [Online]. Available: https://core.ac.uk/download/pdf/235049651.pdf

[2] A. Das, M. R. Kanjilal, M. Mukherjee, and A. Santra, 'Review on Wide Band Gap Semiconductor', in *2022 IEEE International Conference of Electron Devices Society Kolkata Chapter (EDKCON)*, Nov. 2022, pp. 586–591. doi: 10.1109/EDKCON56221.2022.10032898.

[3] X. Liu, J. Huang, Q. Wei, and L. Ye, 'Potential design strategy of wide-bandgap semiconductor p-type β-Ga2O3', *Semicond. Sci. Technol.*, vol. 39, no. 4, p. 043001, Feb. 2024, doi: 10.1088/1361-6641/ad28f2.

[4] J. Zhang, X. Kuang, R. Tu, and S. Zhang, 'A review on synthesis and applications of gallium oxide materials', *Adv. Colloid Interface Sci.*, vol. 328, p. 103175, Jun. 2024, doi: 10.1016/j.cis.2024.103175.

[5] M. Akatsuka *et al.*, 'Preparation of Ga2O3 photocatalyst highly active for CO2 reduction with water without cocatalyst', *Appl. Catal. B Environ.*, vol. 262, p. 118247, Mar. 2020, doi: 10.1016/j.apcatb.2019.118247.

[6] J. Suh and S. D. Tilley, 'Tin Sulfide/Gallium Oxide Heterojunctions for Solar Water Splitting', *Energy Technol.*, vol. 10, no. 1, p. 2100461, 2022, doi: 10.1002/ente.202100461.

[7] F. Shi and H. Qiao, 'Preparations, properties and applications of gallium oxide nanomaterials – A review', *Nano Sel.*, vol. 3, Jul. 2021, doi: 10.1002/nano.202100149.

[8] B. R. Tak *et al.*, 'Recent advances in the growth of gallium oxide thin films employing various growth techniques—a review', *J. Phys. Appl. Phys.*, vol. 54, no. 45, p. 453002, Aug. 2021, doi: 10.1088/1361-6463/ac1af2.

[9] A. Parisini *et al.*, 'Si and Sn doping of ε-Ga2O3 layers', *APL Mater.*, vol. 7, no. 3, p. 031114, Mar. 2019, doi: 10.1063/1.5050982.

[10] M. Pavesi *et al.*, 'ε-Ga2O3 epilayers as a material for solar-blind UV photodetectors', *Mater. Chem. Phys.*, vol. 205, pp. 502–507, Feb. 2018, doi: 10.1016/j.matchemphys.2017.11.023.

[11] J. L. Lyons, 'Electronic Properties of Ga2O3 Polymorphs', *ECS J. Solid State Sci. Technol.*, vol. 8, no. 7, p. Q3226, May 2019, doi: 10.1149/2.0331907jss.

[12] L. Aarik, H. Mändar, A. Kasikov, A. Tarre, and J. Aarik, 'Optical properties of Ga2O3 thin films grown by atomic layer deposition using GaI3 and O3 as precursors', *J. Mater. Chem. C*, vol. 12, no. 28, pp. 10562–10574, Jul. 2024, doi: 10.1039/D4TC01846J.

[13] R.-H. Horng *et al.*, 'Growth mechanism and characteristics of β-Ga2O3 heteroepitaxailly grown on sapphire by metalorganic chemical vapor deposition', *Mater. Today Adv.*, vol. 16, p. 100320, Dec. 2022, doi: 10.1016/j.mtadv.2022.100320.

[14] W. Mi *et al.*, 'Effects of seed layer thickness and post-annealing process on crystalline quality of β-Ga2O3 films prepared on Si (100) substrate by RF magnetron sputtering', *Vacuum*, vol. 214, p. 112235, Aug. 2023, doi: 10.1016/j.vacuum.2023.112235.

[15] X. Liu *et al.*, 'Improved Ga2O3 films on variously oriented Si substrates with Al2O3 or HfO2 buffer layer via atomic layer deposition', *Micro Nanostructures*, vol. 193, p. 207925, Sep. 2024, doi: 10.1016/j.micrna.2024.207925.

[16] G. K. Dalapati *et al.*, 'Tin oxide for optoelectronic, photovoltaic and energy storage devices: a review', *J. Mater. Chem. A*, vol. 9, no. 31, pp. 16621–16684, Aug. 2021, doi: 10.1039/D1TA01291F.

[17] National Center for Biotechnology Information, ‘Tin(IV) oxide’, PubChem. Accessed: May 30, 2025. [Online]. Available: https://pubchem.ncbi.nlm.nih.gov/compound/29011
[18] S. Gul, A. Azam, N. Imrose, S. Riaz, and S. Naseem, ‘Tin Oxide Thin Films Prepared by Sol-gel for PV Applications’, *Mater. Today Proc.*, vol. 2, no. 10, Part B, pp. 5793–5798, Jan. 2015, doi: 10.1016/j.matpr.2015.11.129.
[19] K. Kalam, P. Ritslaid, T. Käämbre, A. Tamm, and K. Kukli, ‘Properties of tin oxide films grown by atomic layer deposition from tin tetraiodide and ozone’, *Beilstein J. Nanotechnol.*, vol. 14, pp. 1085–1092, Nov. 2023, doi: 10.3762/bjnano.14.89.
[20] S. Goldsmith, E. Çetinörgü, and R. L. Boxman, ‘Modeling the optical properties of tin oxide thin films’, *Thin Solid Films*, vol. 517, no. 17, pp. 5146–5150, Jul. 2009, doi: 10.1016/j.tsf.2009.03.019.
[21] N. Bakr, S. Salman, and N. Mohammed, ‘ROLE OF SUBSTRATE TEMPERATURE ON THE STRUCTURAL AND OPTICAL PROPERTIES OF CHEMICALLY SPRAYED SnO 2 THIN FILMS’, *Dig. J. Nanomater. Biostructures*, vol. 14, pp. 517–525, Jul. 2019.
[22] F. Zhang, H. Li, and Q. Guo, ‘Structural and Electrical Properties of Ga2O3 Films Deposited under Different Atmospheres by Pulsed Laser Deposition’, *J. Electron. Mater.*, vol. 47, no. 11, pp. 6635–6640, Nov. 2018, doi: 10.1007/s11664-018-6545-6.
[23] F. Amraoui and N. Sengouga, ‘Ga2O3 deposition methods by low-cost techniques: a review’, *J. Sol-Gel Sci. Technol.*, vol. 111, pp. 1–13, May 2024, doi: 10.1007/s10971-024-06398-6.
[24] S. Wang *et al.*, ‘Effects of growth cycle number and annealing temperature on Ga2O3-on-quartz solar-blind photodetectors’, *Mater. Chem. Phys.*, vol. 306, p. 128037, Sep. 2023, doi: 10.1016/j.matchemphys.2023.128037.
[25] C. V. Ramana *et al.*, ‘Chemical bonding, optical constants, and electrical resistivity of sputter-deposited gallium oxide thin films’, *J. Appl. Phys.*, vol. 115, no. 4, p. 043508, Jan. 2014, doi: 10.1063/1.4862186.
[26] S. Pearton *et al.*, ‘A review of Ga 2 O 3 materials, processing, and devices’, *Appl. Phys. Rev.*, vol. 5, p. 011301, Mar. 2018, doi: 10.1063/1.5006941.
[27] V. L. A. Vijayan, D. Dhanabalan, K. V. Akshita, and S. M. Babu, ‘Investigation of Sn Incorporation in β-Ga2O3 Single Crystals and its Effect on Structural and Optical Properties’, *ECS J. Solid State Sci. Technol.*, vol. 11, no. 10, p. 104003, Oct. 2022, doi: 10.1149/2162-8777/ac9a72.
[28] Y. Shen *et al.*, ‘Atomic-Level Sn Doping Effect in Ga2O3 Films Using Plasma-Enhanced Atomic Layer Deposition’, *Nanomaterials*, vol. 12, no. 23, p. 4256, Nov. 2022, doi: 10.3390/nano12234256.
[29] V. Morari, E. Monaico, V. Zalamai, E. Rusu, and V. Ursaki, ‘Impact of Al and Sn Doping and Annealing Upon Morphology, Wettability and Optical Properties of Ga2O3 Films Prepared by Spray Pyrolysis’, *Romanian J. Phys.*, vol. 70 (1–2), pp. 1–11, Mar. 2025, doi: 10.59277/RomJPhys.2025.70.602.
[30] F. F. Muhammad, M. Y. Yahya, F. Aziz, M. A. Rasheed, and K. Sulaiman, ‘Tuning the extinction coefficient, refractive index, dielectric constant and optical conductivity of Gaq3 films for the application of OLED displays technology’, *J. Mater. Sci. Mater. Electron.*, vol. 28, no. 19, pp. 14777–14786, Oct. 2017, doi: 10.1007/s10854-017-7347-y.
[31] B. G. Streetman and S. K. Banerjee, in *Solid State Electronic Devices*, 6th ed., Pearson Education Inc., p. 81.
[32] J. Ma, J. Lin, J. Liu, F. Li, Y. Liu, and G. Yang, ‘Achieving high conductivity *p*-type Ga2O3 through Al-N and In-N co-doping’, *Chem. Phys. Lett.*, vol. 746, p. 137308, May 2020, doi: 10.1016/j.cplett.2020.137308.

[33] J. Zhang, J. Shi, D.-C. Qi, L. Chen, and K. H. L. Zhang, 'Recent progress on the electronic structure, defect, and doping properties of Ga2O3', *APL Mater.*, vol. 8, no. 2, p. 020906, Feb. 2020, doi: 10.1063/1.5142999.
[34] E. Chikoidze *et al.*, 'Electrical properties of p-type Zn:Ga2O3 thin films', *J. Vac. Sci. Technol. A*, vol. 40, no. 4, p. 043401, May 2022, doi: 10.1116/6.0001766.
[35] H. Zhang *et al.*, 'Growth and physical characterization of high resistivity Fe: β-Ga2O3 crystals*', *Chin. Phys. B*, vol. 29, no. 8, p. 087201, Jul. 2020, doi: 10.1088/1674-1056/ab942d.
[36] M. Orita, H. Hiramatsu, H. Ohta, M. Hirano, and H. Hosono, 'Preparation of highly conductive, deep ultraviolet transparent β-Ga2O3 thin film at low deposition temperatures', *Thin Solid Films*, vol. 411, no. 1, pp. 134–139, May 2002, doi: 10.1016/S0040-6090(02)00202-X.
[37] W. Mi, Z. Li, C. Luan, H. Xiao, C. Zhao, and J. Ma, 'Transparent conducting tin-doped Ga2O3 films deposited on MgAl2O4 (1 0 0) substrates by MOCVD', *Ceram. Int.*, vol. 41, no. 2, Part A, pp. 2572–2575, Mar. 2015, doi: 10.1016/j.ceramint.2014.11.004.
[38] Z. Han *et al.*, 'Transition metal elements-doped SnO2 for ultrasensitive and rapid ppb-level formaldehyde sensing', *Heliyon*, vol. 9, no. 2, p. e13486, Feb. 2023, doi: 10.1016/j.heliyon.2023.e13486.
[39] P. Sivakumar, H. S. Akkera, T. Ranjeth Kumar Reddy, G. Srinivas Reddy, N. Kambhala, and N. Nanda Kumar Reddy, 'Influence of Ga doping on structural, optical and electrical properties of transparent conducting SnO2 thin films', *Optik*, vol. 226, p. 165859, Jan. 2021, doi: 10.1016/j.ijleo.2020.165859.
[40] S. Sujatha Lekshmy and K. Joy, 'Structural and optoelectronic properties of indium doped SnO2 thin films deposited by sol gel technique', *J. Mater. Sci. Mater. Electron.*, vol. 25, no. 4, pp. 1664–1672, Apr. 2014, doi: 10.1007/s10854-014-1781-x.
[41] S. Laghrib, M. Benhaliliba, H. Adnani, and D. Abdi, 'Wide bandgap Indium-doped SnO2 semiconductor prepared by sol-gel route: Multilayer fabrication and Low resistivity for solar cell application', *J. Sol-Gel Sci. Technol.*, vol. 106, no. 2, pp. 530–544, May 2023, doi: 10.1007/s10971-023-06093-y.
[42] O. Bierwagen, T. Nagata, M. E. White, M.-Y. Tsai, and J. S. Speck, 'Electron transport in semiconducting SnO2: Intentional bulk donors and acceptors, the interface, and the surface', *J. Mater. Res.*, vol. 27, no. 17, pp. 2232–2236, Sep. 2012, doi: 10.1557/jmr.2012.172.
[43] P.-P. Filippatos, N. Kelaidis, M. Vasilopoulou, D. Davazoglou, and A. Chroneos, 'Impact of boron and indium doping on the structural, electronic and optical properties of SnO2', *Sci. Rep.*, vol. 11, no. 1, p. 13031, Jun. 2021, doi: 10.1038/s41598-021-92450-2.
[44] A. Mogilatenko *et al.*, 'Effect of heavy Ga doping on defect structure of SnO2 layers', *Phys. Status Solidi A*, vol. 211, no. 1, pp. 87–92, 2014, doi: 10.1002/pssa.201330145.
[45] S. Yasmeen, S. W. Ryu, S.-H. Lee, and H.-B.-R. Lee, 'Atomic Layer Deposition Beyond Thin Film Deposition Technology', *Adv. Mater. Technol.*, vol. 8, no. 20, p. 2200876, 2023, doi: 10.1002/admt.202200876.
[46] R. L. Puurunen, 'Surface chemistry of atomic layer deposition: A case study for the trimethylaluminum/water process', *J. Appl. Phys.*, vol. 97, no. 12, p. 121301, Jun. 2005, doi: 10.1063/1.1940727.
[47] C.-H. Hsu *et al.*, 'Low-temperature spatial atomic layer deposited Ga2O3 films for high-performance flexible deep ultraviolet photodetector', *Mater. Lett.*, vol. 340, p. 134204, Jun. 2023, doi: 10.1016/j.matlet.2023.134204.
[48] J. H. Won, H. Jo, P. J. Youn, B. K. Park, T.-M. Chung, and J. H. Han, 'Ternary Ga–Sn–O and quaternary In–Ga–Sn–O channel based thin film transistors fabricated by plasma-

enhanced atomic layer deposition', *J. Vac. Sci. Technol. A*, vol. 41, no. 6, p. 062406, Oct. 2023, doi: 10.1116/6.0003004.

[49] P. Oviroh *et al.*, 'New Development of Atomic Layer Deposition: Processes, Methods, and Applications', *Sci. Technol. Adv. Mater.*, Apr. 2019, doi: 10.1080/14686996.2019.1599694.

[50] G. N. Parsons *et al.*, 'History of atomic layer deposition and its relationship with the American Vacuum Society', *J. Vac. Sci. Technol. A*, vol. 31, no. 5, p. 050818, Aug. 2013, doi: 10.1116/1.4816548.

[51] R. Johnson, A. Hultqvist, and S. Bent, 'A brief review of atomic layer deposition: From fundamentals to applications', *Mater. Today*, vol. 17, Jun. 2014, doi: 10.1016/j.mattod.2014.04.026.

[52] D. Astrauskytė, K. Galvanauskas, D. Gailevičius, M. Drazdys, M. Malinauskas, and L. Grineviciute, 'Anti-Reflective Coatings Produced via Atomic Layer Deposition for Hybrid Polymer 3D Micro-Optics', *Nanomaterials*, vol. 13, no. 16, Art. no. 16, Jan. 2023, doi: 10.3390/nano13162281.

[53] B. Macco and W. M. M. (Erwin) Kessels, 'Atomic layer deposition of conductive and semiconductive oxides', *Appl. Phys. Rev.*, vol. 9, no. 4, p. 041313, Dec. 2022, doi: 10.1063/5.0116732.

[54] H. Kim, H.-B.-R. Lee, and W.-J. Maeng, 'Applications of atomic layer deposition to nanofabrication and emerging nanodevices', *Thin Solid Films*, vol. 517, no. 8, pp. 2563–2580, Feb. 2009, doi: 10.1016/j.tsf.2008.09.007.

[55] K. Yuan, R. Ma, L. Yang, Y. Yang, and J. Sun, 'Modulation of the dielectric property of Ga2O3/TiO2 nanolaminates and their improvement on the electroluminescence from devices based on Er-doped Al2O3 nanofilms', *J. Phys. Appl. Phys.*, vol. 55, no. 23, p. 235101, Mar. 2022, doi: 10.1088/1361-6463/ac5942.

[56] M. Budde *et al.*, 'SnO/β-Ga2O3 vertical pn heterojunction diodes', *Appl. Phys. Lett.*, vol. 117, no. 25, p. 252106, Dec. 2020, doi: 10.1063/5.0031442.

[57] W. E. Mahmoud, 'Solar blind avalanche photodetector based on the cation exchange growth of β-Ga2O3/SnO2 bilayer heterostructure thin film', *Sol. Energy Mater. Sol. Cells*, vol. 152, pp. 65–72, Aug. 2016, doi: 10.1016/j.solmat.2016.03.015.

[58] D. Walker, 'Analytic Methods for ALD Technologies', Accessed: May 30, 2025. [Online]. Available: https://www.hidenanalytical.com/wp-content/uploads/2024/03/ALD-Analytics-Hiden_edited13thMarch.pdf

[59] M. Junige, M. Geidel, M. Knaut, M. Albert, and J. Bartha, *Monitoring atomic layer deposition processes in situ and in real-time by spectroscopic ellipsometry*. 2011. doi: 10.1109/SCD.2011.6068739.

[60] M. V. Daele, C. Detavernier, and J. Dendooven, 'Surface species during ALD of platinum observed with in situ reflection IR spectroscopy', *Phys. Chem. Chem. Phys.*, vol. 20, no. 39, pp. 25343–25356, Oct. 2018, doi: 10.1039/C8CP03585G.

[61] C. Morales *et al.*, 'In Situ X-Ray Photoelectron Spectroscopy Study of Atomic Layer Deposited Cerium Oxide on SiO2: Substrate Influence on the Reaction Mechanism During the Early Stages of Growth', *Adv. Mater. Interfaces*, vol. 12, no. 5, p. 2400537, 2025, doi: 10.1002/admi.202400537.

[62] D. Longrie, D. Deduytsche, J. Haemers, K. Driesen, and C. Detavernier, 'A rotary reactor for thermal and plasma-enhanced atomic layer deposition on powders and small objects', *Surf. Coat. Technol.*, vol. 213, pp. 183–191, Dec. 2012, doi: 10.1016/j.surfcoat.2012.10.045.

[63] L. Aarik, H. Mändar, J. Kozlova, A. Tarre, and J. Aarik, 'Atomic Layer Deposition of Ga2O3 from GaI3 and O3: Growth of High-Density Phases', *Cryst. Growth Des.*, vol. 23, no. 8, pp. 5899–5911, Aug. 2023, doi: 10.1021/acs.cgd.3c00502.

[64] K. A. Marx, ‘Quartz Crystal Microbalance: A Useful Tool for Studying Thin Polymer Films and Complex Biomolecular Systems at the Solution−Surface Interface’, *Biomacromolecules*, vol. 4, no. 5, pp. 1099–1120, Sep. 2003, doi: 10.1021/bm020116i.

[65] A. K. Mondal, L. K. Ping, M. A. Shazni Mohammad Haniff, M. A. Mohd Sarjidan, B. T. Goh, and M. A. Mohamed, ‘Temperature Dependence of Ultrathin Mixed-Phase Ga2O3 Films Grown on the α-Al2O3 Substrate via Mist-CVD’, *ACS Omega*, vol. 7, no. 2, pp. 2252–2259, Jan. 2022, doi: 10.1021/acsomega.1c05859.

[66] P. Brouwer, ‘Getting acquainted with the principles of XRF’. PANalytical B.V, 2010. Accessed: May 30, 2025. [Online]. Available: https://www.chem.purdue.edu/xray/docs/Theory%20of%20XRF.pdf

[67] R. Sitko and B. Zawisza, ‘Quantification in X-Ray Fluorescence Spectrometry’, 2012. doi: 10.5772/29367.

[68] N. Makeswaran, A. K. Battu, R. Swadipta, F. S. Manciu, and C. V. Ramana, ‘Spectroscopic Characterization of the Electronic Structure, Chemical Bonding, and Band Gap in Thermally Annealed Polycrystalline Ga2O3 Thin Films’, *ECS J. Solid State Sci. Technol.*, vol. 8, no. 7, p. Q3249, Jul. 2019, doi: 10.1149/2.0461907jss.

[69] D. Shiojiri *et al.*, ‘Room-temperature laser annealing for solid-phase epitaxial crystallization of β-Ga2O3 thin films’, *Appl. Phys. Express*, vol. 9, no. 10, p. 105502, Sep. 2016, doi: 10.7567/APEX.9.105502.

[70] E. Makara, ‘Powder XRD’, Aalto University Wiki. Accessed: May 30, 2025. [Online]. Available: https://wiki.aalto.fi/display/SSC/Powder+XRD

[71] A. Karttunen, ‘Grazing incidence XRD’, Aalto University Wiki. Accessed: May 30, 2025. [Online]. Available: https://wiki.aalto.fi/display/SSC/Grazing+incidence+XRD

[72] N. Samsudin, M. F. Omar, and N. S. Rudin, ‘X-Ray Reflectivity Analysis in Evaluating Multilayer Thin Film Fabrication’, *Key Eng. Mater.*, vol. 908, pp. 537–542, Jan. 2022, doi: 10.4028/p-z5v069.

[73] F. Jimenez-Villacorta, ‘Basic Principles of X-ray Reflectivity in Thin Films’, Northeastern University, Feb. 24, 2011. Accessed: May 30, 2025. [Online]. Available: https://www.eng.uc.edu/~beaucag/Classes/Characterization/ReflectivityLab/NorthEastern%20University%20Basic%20Principles%20of%20X-ray%20Reflectivity%20in%20Thin%20Films%20-%20Felix%20Jimenez-Villacorta%20%5BCompatibility%20Mode%5D.pdf

[74] N. Kemik *et al.*, ‘Resonant x-ray reflectivity study of perovskite oxide superlattices’, *Appl. Phys. Lett.*, vol. 99, no. 20, p. 201908, Nov. 2011, doi: 10.1063/1.3660719.

[75] J. B. Cho *et al.*, ‘Highly Asymmetric Optical Properties of β-Ga2O3 as Probed by Linear and Nonlinear Optical Excitation Spectroscopy’, *J. Phys. Chem. C*, vol. 125, no. 2, pp. 1432–1440, Jan. 2021, doi: 10.1021/acs.jpcc.0c08413.

[76] R. K. Ramachandran *et al.*, ‘Plasma enhanced atomic layer deposition of Ga2O3 thin films’, *J. Mater. Chem. A*, vol. 2, no. 45, pp. 19232–19238, Oct. 2014, doi: 10.1039/C4TA05007J.

[77] F. K. Shan, G. X. Liu, W. J. Lee, G. H. Lee, I. S. Kim, and B. C. Shin, ‘Structural, electrical, and optical properties of transparent gallium oxide thin films grown by plasma-enhanced atomic layer deposition’, *J. Appl. Phys.*, vol. 98, no. 2, p. 023504, Jul. 2005, doi: 10.1063/1.1980535.

[78] V. Sharma, *Spectroscopic ellipsometry for the in-situ investigation of atomic layer depositions*. 2014. doi: 10.13140/2.1.2794.8322.

[79] A. T. S. Wee, X. Yin, and C. S. Tang, ‘Introduction to Spectroscopic Ellipsometry of Thin Film Materials: Instrumentation, Data Analysis, and Applications’. WILEY-VCH GmbH, 2022. Accessed: May 30, 2025. [Online]. Available: https://application.wiley-vch.de/books/sample/3527349510_c01.pdf

[80] M. Naftaly *et al.*, 'Sheet Resistance Measurements of Conductive Thin Films: A Comparison of Techniques', *Electronics*, vol. 10, no. 8, Art. no. 8, Jan. 2021, doi: 10.3390/electronics10080960.

[81] 'Four-Probe Method | Sheet Resistance Formula', Ossila. Accessed: May 30, 2025. [Online]. Available: https://www.ossila.com/pages/sheet-resistance-theory

[82] J. Aarik, A. Aidla, A. Jaek, and M. Leskela, 'In situ Study of a Strontium P-Diketonate Precursor for Thinlfilm Growth by Atomic Layer Epitaxy', *J MATER CHEM*, vol. 4, 1994.

[83] J. Aarik, A. Aidla, A. Kasikov, H. Mändar, R. Rammula, and V. Sammelselg, 'Influence of carrier gas pressure and flow rate on atomic layer deposition of HfO2 and ZrO2 thin films', *Appl. Surf. Sci.*, vol. 252, no. 16, pp. 5723–5734, Jun. 2006, doi: 10.1016/j.apsusc.2005.07.067.

[84] L. Aarik, H. Mändar, A. Tarre, H.-M. Piirsoo, and J. Aarik, 'Mechanical properties of crystalline and amorphous aluminum oxide thin films grown by atomic layer deposition', *Surf. Coat. Technol.*, vol. 438, p. 128409, May 2022, doi: 10.1016/j.surfcoat.2022.128409.

[85] L. Aarik *et al.*, 'Atomic layer deposition of high-quality Al2O3 and Al-doped TiO2 thin films from hydrogen-free precursors', *Thin Solid Films*, vol. 565, pp. 19–24, Aug. 2014, doi: 10.1016/j.tsf.2014.06.038.

[86] S. K. Gichana, D. M. Mulati, and T. N. Soitah, 'Structural Characterization of P-type $SnO_2$:Ga and Sb-co-doped $SnO_2$:Ga Thin Films Prepared by Sol-Gel Dip-Coating Method for Potential Optoelectronic Applications', *J. Mater. Phys. Chem.*, vol. 12, no. 2, Art. no. 2, Sep. 2024, doi: 10.12691/jmpc-12-2-3.

[87] Y. Yu, H.-B. Li, W. Li, M. Liu, Y.-M. Zhang, and W. Fei, 'Structure and magnetic properties of magnetron-sputtered FePt/Au superlattice films', *J. Phys. Appl. Phys.*, vol. 41, p. 245003, Nov. 2008, doi: 10.1088/0022-3727/41/24/245003.

[88] H. Yang *et al.*, 'Effects of growth temperature and thickness on structure and optical properties of Ga2O3 films grown by pulsed laser deposition', *Superlattices Microstruct.*, vol. 131, pp. 21–29, Jul. 2019, doi: 10.1016/j.spmi.2019.05.028.

[89] M. Salari Mehr *et al.*, 'Ti doped Cr2O3 thin films: Atomic layer deposition, mechanical and optical properties', *J. Alloys Compd.*, vol. 968, p. 172041, Dec. 2023, doi: 10.1016/j.jallcom.2023.172041.

[90] A. Miglio *et al.*, 'Computed electronic and optical properties of SnO2 under compressive stress', *Opt. Mater.*, vol. 38, pp. 161–166, Dec. 2014, doi: 10.1016/j.optmat.2014.10.017.

[91] Y.-W. Huan *et al.*, 'Recent Advances in β-Ga2O3–Metal Contacts', *Nanoscale Res. Lett.*, vol. 13, Dec. 2018, doi: 10.1186/s11671-018-2667-2.

[92] M.-H. Lee and R. L. Peterson, 'Interfacial reactions of titanium/gold ohmic contacts with Sn-doped β-Ga2O3', *APL Mater.*, vol. 7, no. 2, p. 022524, Feb. 2019, doi: 10.1063/1.5054624.

# Appendices

**Appendix 1**. Cycle composition and the number of cycle repetitions for mixed thin films. G and S represent the cycles of $GaI_3$-$O_3$ and $SnI_4$-$O_3$, respectively.

| Number of cycle repetitions | Cycle composition |
|---|---|
| 24 | 1G-20S / 20G-1S |
| 45 | 1G-10S / 10G-1S |
| 83 | 1G-5S / 5G-1S |
| 125 | 1G-3S / 3G-1S |
| 167 | 1G-2S / 2G-1S |
| 250 | 1G-1S |
| 17 | 20G-10S |
| 22 | 20G-3S |

**Appendix 2**. Design of the shadow mask used for EBE of Ti-Au electrodes. Dimensions are depicted in centimetres.

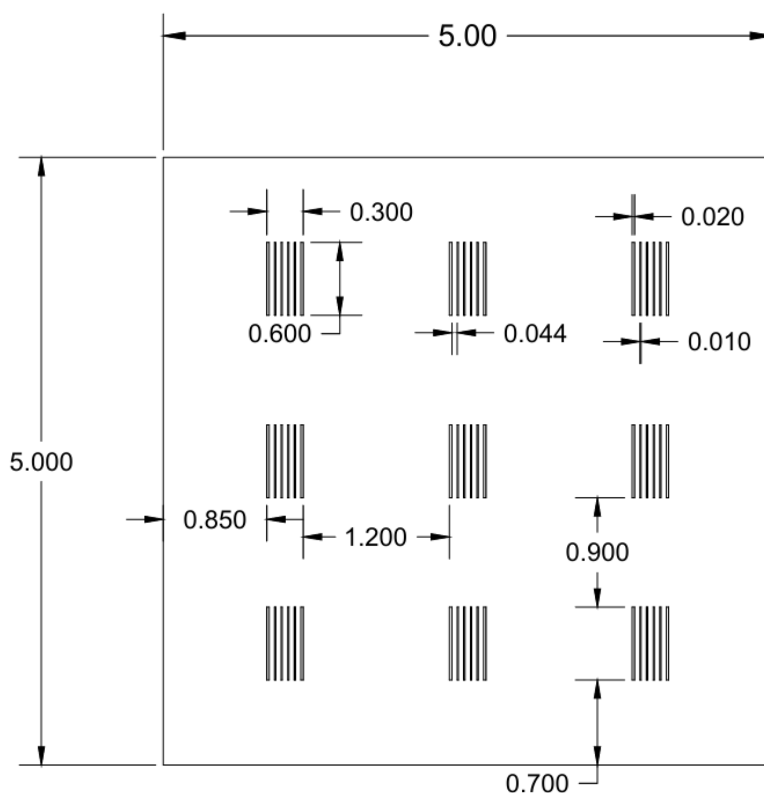

**Appendix 3**. XRR fitting models for (a) doped and (b) superlattice structured films.

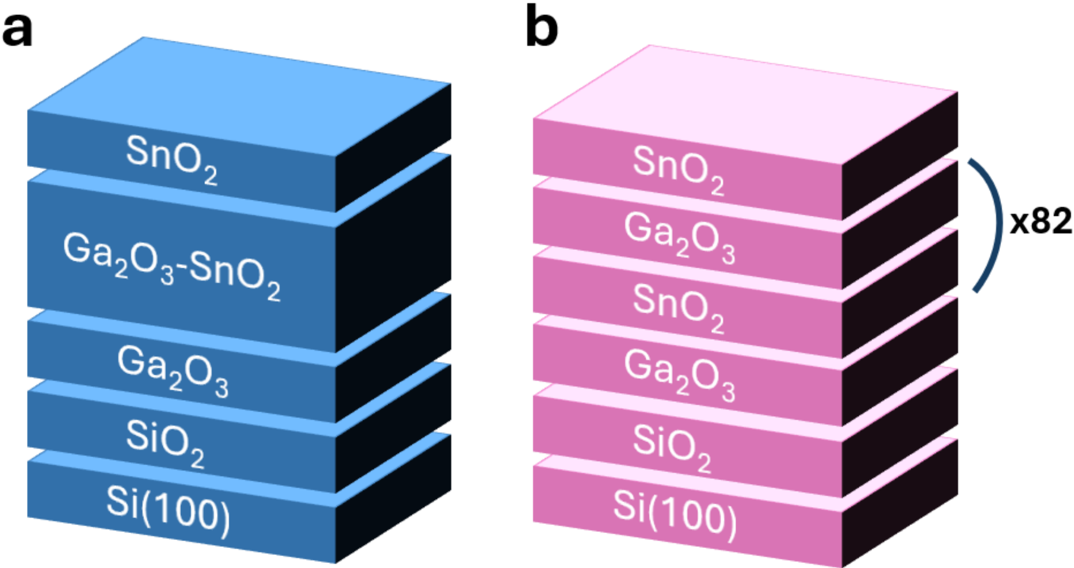


**Appendix 4**. Voltage changes as a function of distance between electrodes. The measured voltage as a function of distance (blue) with trendline (red) showing the electrode resistance.

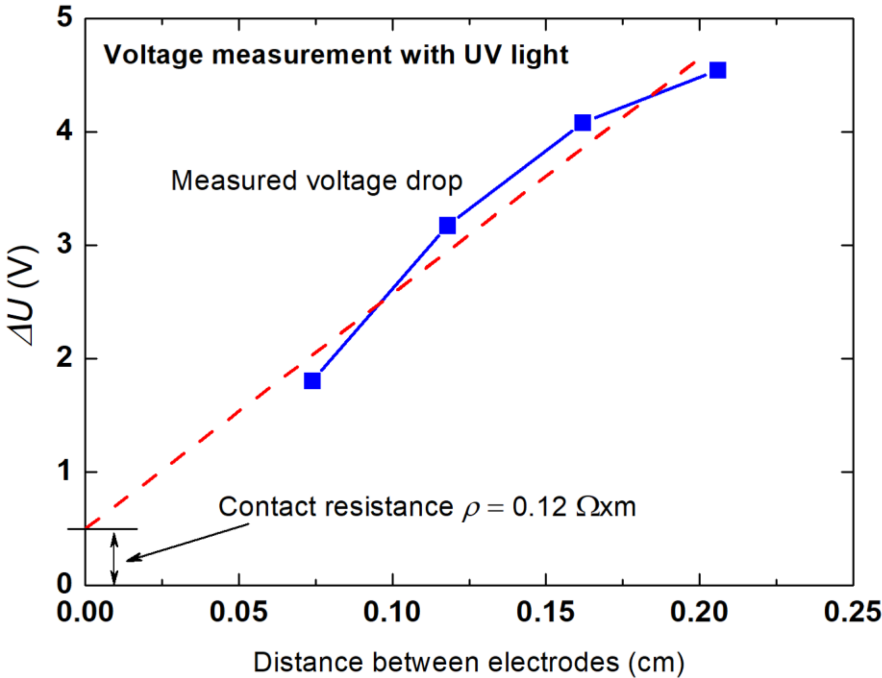

# NON-EXCLUSIVE LICENCE TO REPRODUCE THESIS AND MAKE THESIS PUBLIC

I, **Anna Maria Tuberg**,

1. herewith grant the University of Tartu a free permit (non-exclusive licence) to

reproduce, for the purpose of preservation, including for adding to the DSpace digital archives until the expiry of the term of copyright,

"**Atomic layer deposition and properties of gallium and tin oxide-based thin films**"

supervised by PhD Lauri Aarik and PhD Kaupo Kukli.

2. I grant the University of Tartu a permit to make the work specified in p. 1 available to the public via the web environment of the University of Tartu, including via the DSpace digital archives, under the Creative Commons licence CC BY NC ND 3.0, which allows, by giving appropriate credit to the author, to reproduce, distribute the work and communicate it to the public, and prohibits the creation of derivative works and any commercial use of the work until the expiry of the term of copyright.

3. I am aware of the fact that the author retains the rights specified in p. 1 and 2.

4. I certify that granting the non-exclusive licence does not infringe other persons' intellectual property rights or rights arising from the personal data protection legislation.

*Anna Maria Tuberg*

***30/05/2025***